

Global Biogeochemical Cycles

RESEARCH ARTICLE

10.1029/2020GB006558

Key Points:

- Basin-scale distributions of total dissolvable, dissolved, and labile particulate Cd, Ni, Zn, and Cu in the North Pacific are reported
- Cd is controlled by internal cycling and biological processes, and its stoichiometry with major nutrients is modified via ocean circulation
- The distributions of Ni, Zn, and Cu are affected by scavenging and redissolution from sinking particles and sediments

Supporting Information:

Supporting Information may be found in the online version of this article.

Correspondence to:

L. Zheng,
zheng.linjie.7w@kyoto-u.ac.jp

Citation:

Zheng, L., Minami, T., Takano, S., Ho, T.-Y., & Sohrin, Y. (2021). Sectional distribution patterns of Cd, Ni, Zn, and Cu in the North Pacific Ocean: Relationships to nutrients and importance of scavenging. *Global Biogeochemical Cycles*, 35, e2020GB006558. <https://doi.org/10.1029/2020GB006558>




Received 23 JAN 2020

Accepted 21 MAR 2021

© 2021. The Authors.

This is an open access article under the terms of the [Creative Commons Attribution-NonCommercial-NoDerivs License](https://creativecommons.org/licenses/by-nc-nd/4.0/), which permits use and distribution in any medium, provided the original work is properly cited, the use is non-commercial and no modifications or adaptations are made.

Sectional Distribution Patterns of Cd, Ni, Zn, and Cu in the North Pacific Ocean: Relationships to Nutrients and Importance of Scavenging

Linjie Zheng¹ , Tomoharu Minami², Shotaro Takano¹, Tung-Yuan Ho^{3,4} , and Yoshiaki Sohrin¹ 

¹Institute for Chemical Research, Kyoto University, Uji, Japan, ²Engineering and Technology Department, Kanazawa University, Kanazawa, Japan, ³Research Center for Environmental Changes, Academia Sinica, Taipei, Taiwan, ⁴Institute of Oceanography, National Taiwan University, Taipei, Taiwan

Abstract The North Pacific Ocean is located at the end of the thermohaline circulation of deep water. This study reports on basin-scale full-depth sectional distributions of total dissolvable (td), dissolved (d), and labile particulate (lp) Cd, Ni, Zn, and Cu along three transects: the GEOTRACES transects GP18 (165°E) and GP02 (47°N), and along 160°W. We find that scavenging is an important factor that significantly affects the distributions of dZn, dNi, and dCu, of which the magnitude of influence increases in the order of Cd < Ni, Zn < Cu. The relationships between the four dissolved metals with Si(OH)₄ and PO₄ differed considerably from those in other oceans. The spot concentration ratio of dCd/PO₄ was 0.34 ± 0.02 nmol/μmol ($n = 296$) in waters >800 m deep, which is in the range of the phytoplankton Cd/P ratio. This is indicative of the dominant effect of water circulation and biological processes on dCd distribution. The dissolved metals (dMs) to PO₄ ratios of other examined metals were either partially or completely outside the range of typical biomass ratios. They generally increased with depth in waters >800 m deep; the magnitude of increase was the highest for Cu and moderate for Ni and Zn. Below 800 m, an increase in the apparent oxygen utilization from 150 to 300 μmol/kg was concurrent with a decrease in the dMs/PO₄ ratios: $4 \pm 3\%$ for Cd, $21 \pm 4\%$ for Zn, $21 \pm 3\%$ for Ni, and $69 \pm 7\%$ for Cu.

1. Introduction

Trace metals with nutrient-type distributions are actively taken up by phytoplankton in surface waters. They then sink to depths with sinking particles and are released from particles via the oxidative decomposition of organic matter and the dissolution of minerals, such as silica and carbonates (Broecker & Peng, 1982; Elderfield, 2003). Cadmium (Cd), nickel (Ni), zinc (Zn), and copper (Cu) are classified as nutrient-type or recycled-type trace metals (Bruland et al., 1994; Whitfield & Turner, 1987). These metals are essential cofactors in metalloenzymes and thus control the metabolism of organisms (Sunda, 1989; Twining & Baines, 2013). In turn, the oceanic phytoplankton community significantly affects the concentration and cycling of trace metals in the ocean (Sunda, 2012).

The concentrations of nutrient-type metals in deep water (>1500 m in depth) generally increase with the age of deep water from the Atlantic Ocean through the Southern Ocean and ultimately to the Indian and Pacific Oceans (Table 1). In addition, the concentration of dissolved Cu (dCu) increases from surface to bottom by almost five times in the Pacific Ocean (Bruland, 1980), while this increase is only 10% in the Atlantic Ocean (Danielsson et al., 1985). Oceanic circulation affects not only the concentrations of the nutrient-type metals but also their ratios against major nutrients (Table 1). This study used the metal to nutrient concentration ratio in a given sample (metal/nutrient) to indicate the spot concentration ratio (e.g., dCd/PO₄) and metal:nutrient (e.g., Cd:PO₄) to indicate the slope of a regression line in metal versus nutrient plots. This slope indicates an uptake ratio or a remineralization ratio as per the definition reported in the literature (Middag et al., 2018; Quay et al., 2015). The dCd/PO₄ in deep water exhibits significant spatial variations (Löscher et al., 1998; van der Loeff et al., 1997); it is ~0.24 nmol/μmol in the North Atlantic Ocean and ≥0.3 nmol/μmol in other oceans (Table 1). Alternatively, this difference in the dCd/PO₄ ratio may also be due to Cd regeneration from different ballasts of sinking biogenic particles. The Cd/PO₄ ratio of silica ballast in the North Pacific is presumed to be higher than the CaCO₃ ballast in the North Atlantic (Wu & Roshan, 2015).

Table 1
dCd, dNi, dCu, and dZn Concentrations and Their Ratios to Phosphate in the Global Ocean at Depth > 1,500 m^a

>1500 m	Unit	North Atlantic Ocean			South Atlantic Ocean			Southern Ocean			Indian Ocean			South Pacific Ocean			North Pacific Ocean		
		ave	sd	n	ave	sd	n	ave	sd	n	ave	sd	n	ave	sd	n	ave	sd	n
dCd	nmol/kg	0.27 ± 0.10	0.62 ± 0.17	441	0.76 ± 0.06	84	0.84 ± 0.10	37	0.81 ± 0.07	439	0.92 ± 0.08	369							
dNi	nmol/kg	4.37 ± 0.50	6.73 ± 1.39	373	7.13 ± 0.26	24	8.46 ± 0.84	37	8.40 ± 0.71	421	9.59 ± 0.43	352							
dCu	nmol/kg	1.79 ± 0.46	2.61 ± 0.86	212	2.52 ± 0.35	61	3.44 ± 1.03	37	3.28 ± 0.77	455	3.11 ± 0.67	350							
dZn	nmol/kg	2.30 ± 1.01	5.37 ± 2.08	479	7.12 ± 2.54	66	8.36 ± 1.25	37	7.55 ± 1.42	433	9.92 ± 0.68	308							
Cd/PO ₄	nmol/μmol	0.24 ± 0.02	0.30 ± 0.03	431	0.35 ± 0.02	60	0.36 ± 0.04	37	0.32 ± 0.02	348	0.35 ± 0.02	219							
Ni/PO ₄	nmol/μmol	3.44 ± 0.19	3.34 ± 0.21	373	-	-	3.64 ± 0.47	37	3.35 ± 0.17	351	3.62 ± 0.19	220							
Cu/PO ₄	nmol/μmol	1.32 ± 0.29	1.19 ± 0.27	212	1.12 ± 0.18	37	1.48 ± 0.47	37	1.30 ± 0.29	364	1.21 ± 0.33	218							
Zn/PO ₄	nmol/μmol	1.58 ± 0.43	2.60 ± 0.71	478	2.49 ± 0.40	42	3.59 ± 0.54	37	3.12 ± 0.37	332	3.70 ± 0.21	134							

^aData from GEOTRACES Intermediate Data Product 2017 and this study.

Notably, seawater concentrations of dissolved metals (dMs) and their relationships with major nutrients in different ocean basins cannot be fully described using only oceanic water circulation. For instance, Ni is a known cofactor in the enzyme urease for phytoplankton to obtain nitrogen and carbon dioxide from urea (Morel et al., 2003; Sunda, 1989). As such, the colimitation of Ni and NO₃ on phytoplankton growth has been proposed (Bruland et al., 1991; Price & Morel, 1991). Unlike other nutrient-type metals, the surface concentration of dNi never decreases below 1.8 nmol/kg (Boyle et al., 1981; Bruland, 1980; Danielsson et al., 1985; Wang et al., 2019), and it has been postulated that this residual surface Ni is nonbioavailable (Mackey et al., 2002). Recently, there were reports that the high surface dNi in the South Atlantic Ocean has a heavy isotope signature with a fractionation factor of 0.99965 in a simple closed-system Rayleigh fraction model (Archer et al., 2020). This suggests the potential preferential removal of isotopically light Ni via scavenging to particulate matter and/or by biological uptake.

Boyle et al. (1977) reported full-depth profiles of total Cu, using unfiltered seawater in the central North Pacific Ocean, with a surface maximum of approximately 3 nmol/kg and a monotonic increase to the bottom. They suggested that this unique distribution was maintained by aeolian input to ocean surface waters, ubiquitous scavenging in the subsurface and deep water, and a strong bottom source. The linear distribution of dCu with depth may be attributed to reversible scavenging between dissolved and suspended particulate (p) species (Little et al., 2013). A sediment trap experiment in the North Pacific Ocean demonstrated that approximately 65% of the total Cu flux in the deepest trap (~3000 m) had been derived from primary flux from the upper water, resuspension, and hydrothermal inputs. In contrast, the source of the remaining 35% of total Cu had not been clarified and was considered residual flux input, implying the coexistence of alternative processes (Fischer et al., 1986). The authors attributed this residual to the lateral transport of particles or the readsorption of dCu released from bottom sediments. A recently developed box model, based on the isotope ratios and concentrations of dCu, confirmed the release of dCu from the upper sedimentary layers during early diagenesis (Takano et al., 2014).

The vertical distribution of dCd is close to that of PO₄, exhibiting a linear relationship over oceans worldwide (Boyle et al., 1976; Bruland, 1980; Roshan & Wu, 2015a; Zhang et al., 2019) (Figure 1a). However, a slope-change, which is denoted as a “kink,” was observed in the North Atlantic upper waters (where PO₄ was <1.3 μmol/kg), and the South Atlantic and Pacific waters (where PO₄ > 1.3 μmol/kg) (Boyle, 1988). The linear relationship in deep waters is indicative of the dominant effects of water mass mixing on dCd distribution in the North Atlantic (Quay et al., 2015), the South Atlantic (Xie et al., 2015), and the Southern Oceans (Baars et al., 2014). The water mass mixing, however, cannot explain a relatively low slope in the surface-to-subsurface waters, and many hypotheses have been proposed. Elderfield and Rickaby (2000) proposed a preferential uptake of Cd over PO₄ by phytoplankton in surface water, particularly under iron-limited conditions in high-nutrient and low-chlorophyll (HNLC) areas (Cullen, 2006; Quay et al., 2015). The dCd versus PO₄ regression line in the North Pacific was linear throughout the water column, differing from that observed in other oceans (Bruland, 1980; de Baar et al., 1994) (Figure 1a). Furthermore, a decoupling of dCd and PO₄ revealing a relative depletion of dCd was observed in the oxygen minimum zone (OMZ) in the eastern North Pacific and North Atlantic Oceans (Janssen et al., 2014). In this instance, suspended particles were enriched with lighter isotopes of Cd (Conway & John, 2015). These results were interpreted based on the precipitation of CdS in a euxinic microenvironment around sinking particles. In contrast, Wu and Roshan (2015) did not observe dCd depletion in the sectional distribution of dCd/PO₄ in OMZ in the North Atlantic, although there was a dCd depletion relative to PO₄ in the dCd versus PO₄ plot. The observed depletion was ascribed to a low dCd/PO₄ ratio in shallow seawater and the enhanced regeneration of the low dCd/PO₄ ratio in the OMZ.

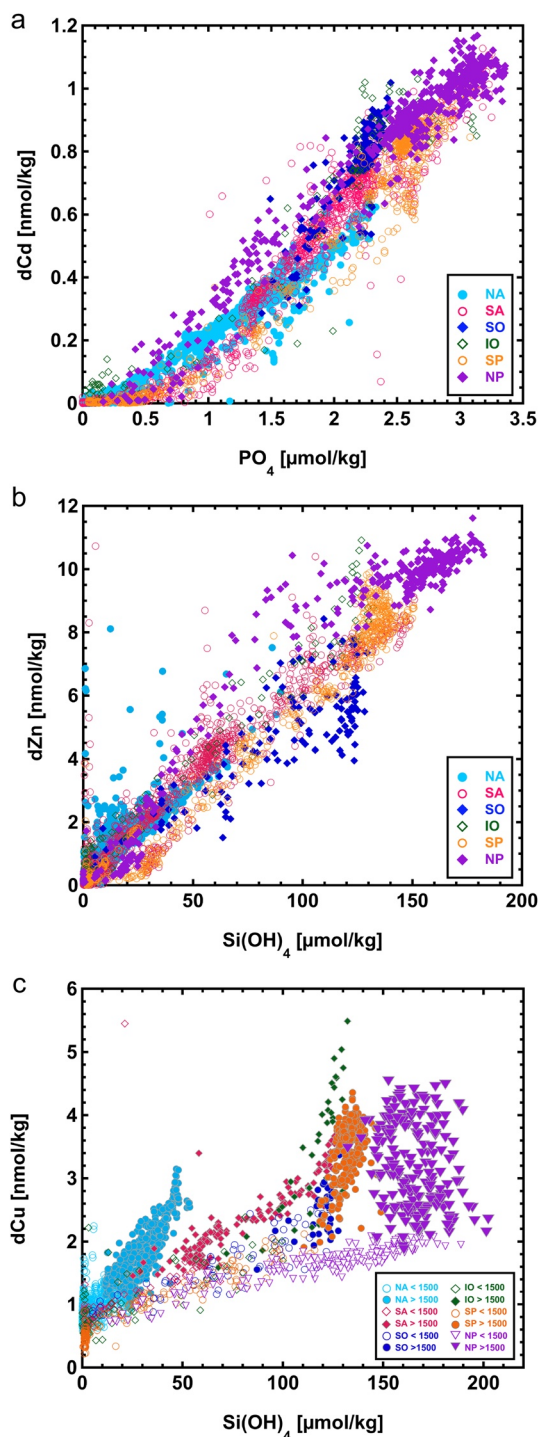


Figure 1. Compiled global data of (a) dCd versus PO_4 ; (b) dZn versus $Si(OH)_4$, and (c) dCu versus $Si(OH)_4$. Blue circles: the North Atlantic Ocean (NA), pink circles: the South Atlantic Ocean (SA), dark blue diamonds: the Southern Ocean (SO), green diamonds: the Indian Ocean (IO), yellow circles: the South Pacific Ocean (SP), purple diamonds: the North Pacific Ocean (NP). Data are derived from GEOTRACES Intermediate Data Product 2017 (Schlitzer et al., 2018) and this study.

The strong correlation between dZn and $Si(OH)_4$ in oceans worldwide is another example of the relationship between metals and major nutrients (Bruland, 1980; Janssen & Cullen, 2015; Kim et al., 2017; Roshan et al., 2018; Vance et al., 2017; Wang et al., 2019) (Figure 1b). Ocean circulation from the Southern Ocean is suggested to play an important role in dZn distribution (Vance et al., 2017). However, decoupling of the dZn versus $Si(OH)_4$ relationship occurs in intermediate waters, where many points are located above the regression line across oceans worldwide (Janssen & Cullen, 2015; Vance et al., 2019; Vance et al., 2017; Wyatt et al., 2014). Janssen and Cullen (2015) proposed that the relationship between Zn and $Si(OH)_4$ in the eastern North Pacific Ocean is divided into two parts, the oxygenated upper waters and the relatively low oxygen deep waters, which may be ascribed to preferential removal of ZnS. In contrast, Vance et al. (2019) considered this distribution to be a result of the preferential regeneration of dZn in shallow waters and the preferential dissolution of silica in deep waters. The observed slope of dZn: $Si(OH)_4$ in the Pacific and Atlantic Oceans is approximately 0.06 nmol/ μ mol (Schlitzer et al., 2018). Zn uptake experiments using *Thalassiosira pseudonana*, a marine diatom, indicates that only 1–3% of cellular Zn was incorporated into the silica frustule. Additionally, it was found that the dissolution of the silica resulted in a regeneration ratio of $0.3\text{--}3.2 \times 10^{-3}$ nmol/ μ mol (Ellwood & Hunter, 2000). This means that diatom silica is not a major mechanism controlling dZn distribution. The scavenging of nutrient-type metals in deep waters is considered to be negligible (Elderfield, 2003). However, alongside the principle role of water circulation, model calculations have demonstrated the crucial role of reversible scavenging of Zn on sinking particles (Weber et al., 2018).

The interaction of dMs with seawater particles is proposed as a major factor governing trace metal distribution in oceans around the world (Goldberg, 1954; Sherrell & Boyle, 1992). As such, a series of recent studies have focused on the role of scavenging on dZn and dCu (John & Conway, 2014; Little et al., 2013; Weber et al., 2018). At VERTEX-IV ($28^\circ N$, $155^\circ W$) in the eastern North Pacific, suspended particulate Cd (suspended pCd) concentration decreased from 2.5 to 0.2 pmol/kg below 90 m depth, while the pZn concentration was 8 and 80 times higher, respectively (Bruland et al., 1994); this is indicative of the higher intrabasin enrichment of Zn. Concentrations of suspended pCd and pZn were enriched in the North Pacific Ocean compared with the North Atlantic Ocean, suggesting an enhanced association of dMs with particles (Bruland et al., 1994; Sherrell & Boyle, 1992). Sediment trap experiments conducted at four stations in the Antarctic and the North Pacific Oceans demonstrated that pCd flux increased with the total particulate flux, while the flux for pNi and pCu did not depend on the total particulate flux (Noriki & Tsunogai, 1992). These findings were attributed to different carrier particles. The pNi and pCu are suggested to have been transferred by nonbiogenic inorganic and biogenic particles, while pCd is almost entirely transferred from the latter. Despite this existing research, there are limited data on the four nutrient-type metal concentrations in suspended and sinking particles in the Pacific Ocean (Bruland et al., 1994; Janssen et al., 2019; Noriki & Tsunogai, 1992; Yang et al., 2018).

This study reports the concurrent and basin-scale sectional distributions of total dissolvable (td), dissolved (d), and labile particulate (lp) species of nutrient-type trace metals (Cd, Ni, Zn, and Cu) in the North Pacific

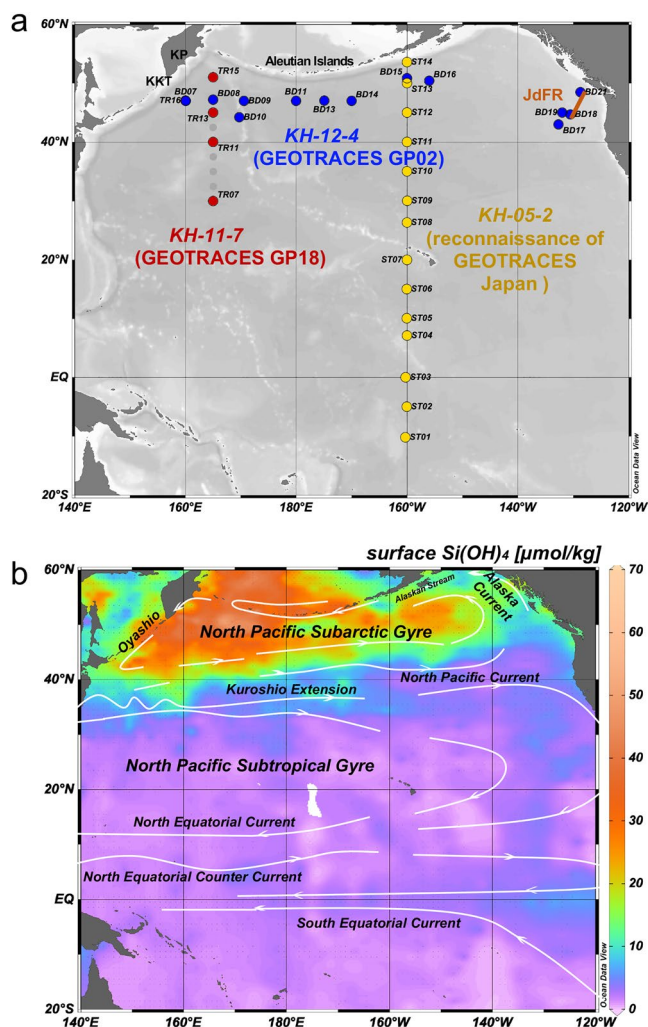


Figure 2. Maps of (a) sampling stations and (b) hydrography in the North Pacific Ocean. White solid lines and brown line represent surface currents and the Juan de Fuca Ridge (JdFR), respectively. KP, KKT in (a) represent the Kamchatka Peninsula and the Kuril-Kamchatka Trench, respectively. The background color represents the annually averaged surface $\text{Si}(\text{OH})_4$ concentrations in 2013 derived from the World Ocean Atlas V2 2013 (www.nodc.noaa.gov).

Ocean. This was carried out to elucidate major factors that control their distribution and their relationship with the major nutrients, PO_4 and $\text{Si}(\text{OH})_4$. Data referring to other metals were also used for discussion (Zheng & Sohrin, 2019; Zheng et al., 2019). The concurrent observation of trace metals will aid in enhancing the current understanding of scavenging and other processes of nutrient-type trace metals.

2. Materials and Methods

2.1. Materials and Sampling

Clean samples of trace metals were collected during the three GEOTRACES cruises onboard the research vessel Hakuho Maru: this included KH-05-2, from August to September 2005, KH-11-7 in July 2011, and KH-12-4 from August to September 2012 (Figure 2). The details of the materials used and sampling methods are reported in previous studies (Zheng & Sohrin, 2019; Zheng et al., 2017, 2019). The KH-05-2 cruise (along 160°W , 10°S – 54°N) was a reconnaissance study by GEOTRACES Japan. The KH-11-7 and KH-12-4 cruises were arranged for formal studies of GEOTRACES Japan, occupying the GEOTRACES sections of GP18 (along 165°E , 30°N – 51°N), and GP02 (160°E – 129°W , along 47°N), respectively. Samples (~ 125 g) used to determine the total dissolvable trace metals (tdMs) were unfiltered and acidified to pH 2.2 using ultrapure HCl (TamaPure AA-10, Tama Chemicals) immediately after collection. Portions of collected seawater samples were filtered onboard using $0.2 \mu\text{m}$ filters to acquire the dM samples. Nuclepore polycarbonate membrane filters (Whatman) were used for the KH-05-2 and KH-11-7 cruises, while during the KH-12-4 cruise, AcroPak capsule filters (Pall) were utilized. These filtered seawater samples were also acidified to pH 2.2 with ultrapure HCl. Seawater samples were stored at room temperature for at least one year prior to analysis. The difference between tdM and dM concentrations was defined as the labile particulate trace metal (lpM) concentration, which represented components liberated from particulate phases during sample storage at pH ~ 2.2 . The concentrations of dZn and tdZn from the KH-05-2 cruise were removed from the dataset because of contamination from the sacrificial Zn electrode attached to the seawater sampling system. Ocean Data View software was used for data analysis and the preparation of figures (Schlitzer, 2015).

2.2. Analytical Methods

An offline automated solid-phase extraction system (SPE-100, Hiranuma Sangyo) with a column of Nobias Chelate-PA1 resin (Hitachi High-Technologies) was used to preconcentrate the trace metals (Al, Mn, Fe, Co, Ni, Cu, Zn, Cd, and Pb) in seawater (Minami et al., 2015). A detailed description of the applied analytical methods is provided in previous studies (Zheng & Sohrin, 2019; Zheng et al., 2019). The collected seawater samples were adjusted to pH 6.00 ± 0.05 , in a clean room (class 1000), and immediately introduced into the SPE-100 system. Procedural blanks were measured using ultrapure water prior to the analyses of seawater samples. A high-resolution inductively coupled plasma mass spectrometer (HR-ICP-MS, Element 2, Thermo Fisher Scientific), was used to determine trace metal concentrations using the calibration curve method.

A series of certified reference materials for trace metals CASS-5, 6 and NASS-6, 7 and the GEOTRACES open-ocean reference samples (GS, GD, GSP, and GSC) were measured to ensure the accuracy of the applied method (Table S1). Concentrations of dNi, dZn, and dCd were in good agreement with the certified and/or consensus values, while dCu concentrations were only in line with the certified values of CASS

and NASS, which were gamma-irradiated. dCu concentrations were 65%–89% of consensus values for the GEOTRACES reference samples (GS, GD, GSP, and GSC). These consensus values were obtained following ultraviolet (UV) irradiation (Buck & Bruland, 2005; Lohan et al., 2005), while the samples in this study were not subjected to UV irradiation. This means that a portion of dCu that forms strong complexes with organic ligands may not be measurable. UV irradiation was not applied in this study as it may lead to the unexpected contamination of some metals (Zheng et al., 2019), and the data obtained for Cu in this study were considered sufficiently reproducible.

Table S2 summarizes the procedural blanks and detection limits (DLs) for all species. The DL for tDMs and dMs samples was calculated as three times the standard deviation (sd) of the procedural blank. Based on the analysis of reference materials, the relative standard deviation was ~5% for each metal (Table S1), DL for lPMs were defined using the equation $2 \times \sqrt{2} \times 0.05 \times C_{\text{ave}}$, considering the propagation of uncertainty. Here C_{ave} represents the average concentration of dMs. In this study, not detected (ND) data below the DL were assigned a value of $DL \times (1 / \sqrt{2})$ for further analysis and preparation of figures, when the number of ND was <50% of the data (Croghan & Egeghy, 2003).

2.3. Cross-Over Stations

Cross-over stations stipulated by GEOTRACES provide a measure of data consistency (<http://www.geotraces.org>). Stations TR16 from GP18 and BD07 from GP02 were located at the same position (160°E, 47°N) and served as internal cross-over stations (Figure S1). The vertical profiles of dMs and PO₄ fitted well between BD07 and TR16 within the expected range of analytical uncertainty (Figure S1). All regression lines of dMs in plots of BD07 versus TR16 had a coefficient of determination (r^2) higher than 0.90 (Table S3), with negative intercepts. The surface water at BD07 had a lower salinity, higher temperature, and lower nutrient concentration than TR16; this suggests a stronger influence from the Kuroshio Waters. For waters ≥ 200 m deep, the values of r^2 and slopes of the regression lines approached 1, with the exception of Zn (Table S3).

Stations ST13 (160°W, 50°N) and ST14 (160°W, 54°N) from the KH-05-2 cruise were located 100 km south and 300 km north of station BD15 (160°W, 51°N) of GP02, respectively (Figure S2). Although the three stations were not strict cross-over stations, we used vertical profiles at these stations for intracomparison. The vertical profiles of dMs and PO₄ fitted well for the ST13, ST14, and BD15 stations within the expected range of analytical uncertainty (Figure S2). All regression lines between ST13 and BD15 had r^2 values higher than 0.96 (Table S3). The concentrations of dNi, dCd, Si(OH)₄, and PO₄ in surface water were lower at BD15 than at ST13. This may be due to a higher chlorophyll *a* (Chl. *a*) content that enables the higher uptake of Ni, Cd, and nutrients (Figure S2c). Previous studies have reported that the concentrations of Al, Mn, and Fe substantially decreased from ST14 to ST13, due to boundary scavenging (Zheng & Sohrin, 2019; Zheng et al., 2019). However, no apparent concentration gradients were observed in this study, revealing that boundary scavenging does not significantly affect the distribution of nutrients and nutrient-type trace metals. Only dCu exhibited a surface maximum at ST14 (Figure S2b), where the Alaskan Stream flowed and the surface maxima of tDMn and tDCo occurred (Zheng et al., 2019).

3. Results

3.1. Hydrography

3.1.1. Surface Currents and Water Masses

Figure 2a presents the sampling stations in this study, and Figure 2b presents the annually averaged surface Si(OH)₄ concentrations from the World Ocean Atlas V2 2013 (www.nodc.noaa.gov). The white solid lines in Figure 2b denote the surface currents. The Oyashio Current, North Pacific Current, Alaska Current, and Alaskan Stream form the anticlockwise upwelling North Pacific Subarctic Gyre (NPSAG) to the north of 40°N. The North Pacific Subtropical Gyre (NPSTG) to the south of the Subarctic Front consists of the Kuroshio Extension, North Pacific Current, and North Equatorial Current (Yuan & Talley, 1996), where inorganic phosphate concentrations are extremely low.

There are two mode waters, two central water masses, and three intermediate water masses in the upper 1000 m of the study area (Figure S3a). The two mode waters are the South Pacific Subtropical Mode Water (SPSTMW) and the North Pacific Subtropical Mode Water (NPSTMW); the former is denser than the latter with a core salinity of 35.5 (Talley et al., 2011). The two central waters are the North Pacific Central Water (NPCW) and the South Pacific Central Water (SPCW); the former extends northward from the equator to $\sim 40^\circ\text{N}$, while the latter extends southward from $\sim 10^\circ\text{S}$ to $\sim 55^\circ\text{S}$ (Talley et al., 2011). The intermediate water masses comprise the North Pacific Intermediate Water (NPIW), the Antarctic Intermediate Water (AAIW), and the Equatorial Pacific Intermediate Water (EqPIW). The former originates from the Okhotsk Sea Mode Water (OSMW), which is formed to the east of Hokkaido, Japan and spreads to the southeast (Talley, 1993). NPIW is characterized by low salinity and density with a potential density anomaly (σ_θ) of 26.4–27.2 kg/m³ (average: 26.8) (Yasuda, 1997). AAIW originates from the north of the Subantarctic Front (Bostock et al., 2010; Talley et al., 2011) and extends to $\sim 15^\circ\text{N}$ in the tropical–subtropical transition (Talley et al., 2011). EqPIW is formed by a combination of AAIW and the Pacific Deep Water (PDW). Among the three water masses, NPIW is the shallowest (200–800 m in depth), followed by EqPIW (700–1000 m in depth) and AAIW (600–1100 m in depth) (Bostock et al., 2010; Talley et al., 2011). The stations to the north of 40°N in the subarctic gyre are influenced by the Dichothermal Water (DtW) and the California Current System Water (CCSW).

Two distinct deep waters exist in the North Pacific Ocean: the Circumpolar Deep Water (CDW) and the PDW. The upper CDW (UCDW) and lower CDW (LCDW) are two branches of the CDW, formed by the mixing of the North Atlantic Deep Water and other deep waters in the Southern Ocean. PDW is formed internally in the North Pacific by mixing upwelled bottom waters with the UCDW. The PDW and UCDW appear in almost the same density range, while UCDW flows northward and PDW flows southward (Talley et al., 2011). LCDW flows at the maximum depth into the Pacific Ocean and is characterized by a high salinity of 34.72.

3.2. Relationship Among Major Nutrients

Figure S4 presents the horizontal distribution of the major nutrients, dCd/PO₄, and Chl. *a*. The concentration of Si(OH)₄ in the surface water was ~ 25 $\mu\text{mol}/\text{kg}$ in the Western Subarctic Gyre (WSG), and almost zero in the subtropical gyre and around the Juan de Fuca Ridge (JdFR) (Figure S4a). The surface concentrations of PO₄ and NO₃ exceeded 0.5 and 7 $\mu\text{mol}/\text{kg}$ in NPSAG, respectively; this is known as one of the HNLC regions (Figures S4d and S4g). At ST14, closest to the Aleutian Islands, the surface concentrations of major nutrients were extremely low, where Chl. *a* reached a maximum of 2.7 $\mu\text{g}/\text{kg}$ (Figure S4l).

Figures S3b–S3d present tracer–tracer plots of major nutrients. The relationships between Si(OH)₄ and PO₄, and Si(OH)₄ and NO₃ were characterized by lower slopes in the upper 800 m (PO₄ < 3.0 $\mu\text{mol}/\text{kg}$, NO₃ < 42.4 $\mu\text{mol}/\text{kg}$) at stations to the south of the North Equatorial Current (ST01–ST06, 10°S – 15°N) compared with northern stations. These results signify the dominant effects of the SPCW, AAIW, EqPIW, and SPSTMW at the southern stations. In contrast, the relationships between Si(OH)₄ and PO₄, and NO₃ and PO₄ were characterized by slightly higher slopes in the upper 800 m waters at stations from 20°N – 40°N in the subtropical gyre compared with northern stations located to the north of 40°N in the subarctic gyre. This may be attributable to the effects of NPIW, NPCW, and NPSTMW. In deep waters, there were no linear relationships between Si(OH)₄ and PO₄, and Si(OH)₄ and NO₃, while NO₃ and PO₄ exhibited a linear relationship throughout the study area (Figure S3d).

3.3. Distributions of Trace Metals

Table S4 presents the statistical summary of tDMs, dMs, and lpMs. The full-depth sectional distributions of dMs from the KH-05-2, GP02, and GP18 cruises are presented in Figure 3. Figure 4 illustrates the horizontal distributions of dMs, at depth first (10–20 m in depth), at $\sigma_\theta = 26.8$ kg/m³, the mean σ_θ of NPIW, and at a depth of 4500 m where LCDW flows. In general, the dMs distributions were similar to those of the major nutrients. However, each dM had distinct characteristics, as described below.

The dCd exhibited correlation coefficients (*r*) higher than 0.98, for PO₄ and NO₃ for all data (Table S5). In contrast to PO₄ and NO₃, a maximum dCd occurred at a depth of 200–500 m in stations to the north of

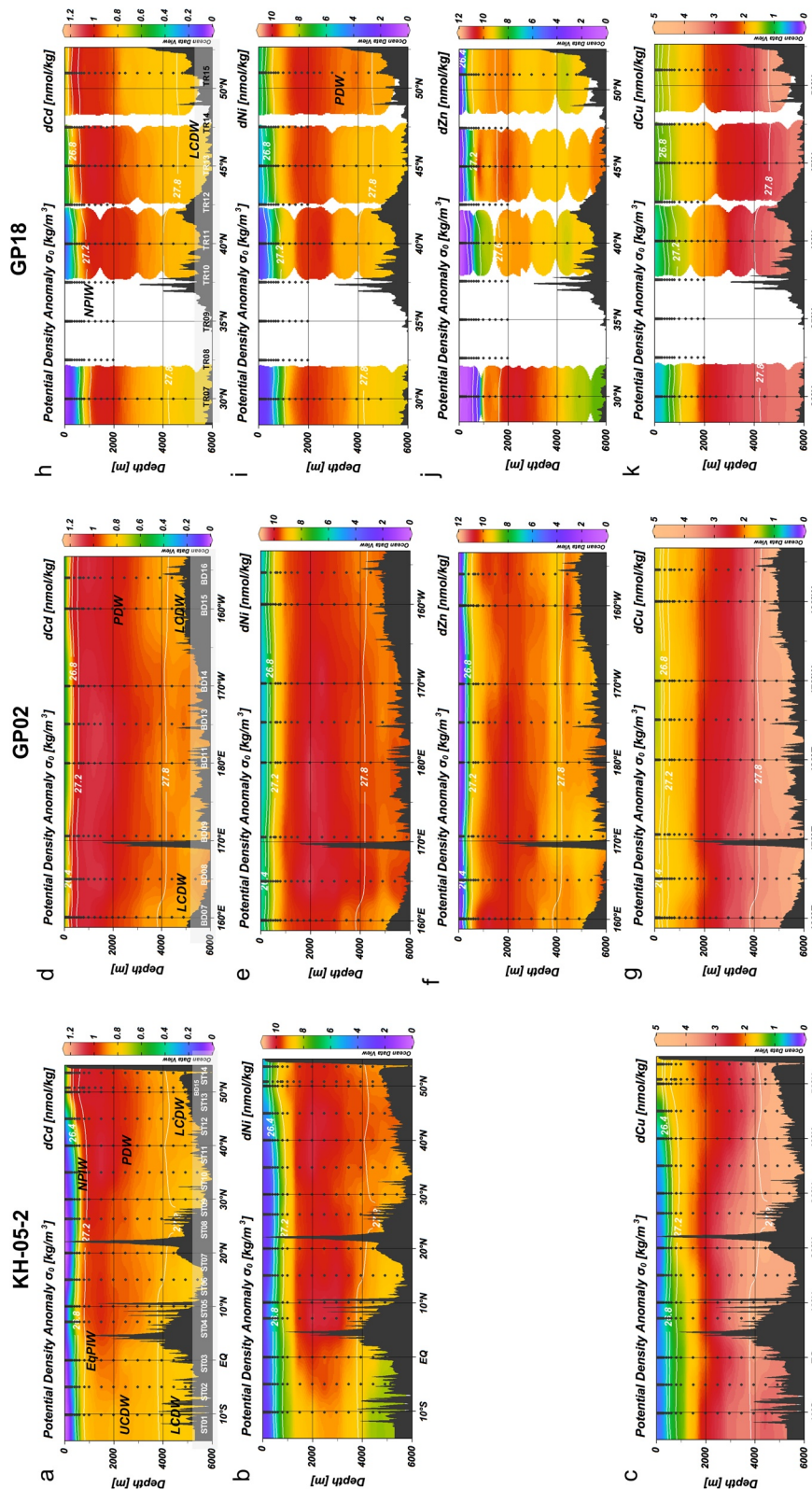


Figure 3. Full-depth sectional distribution of (a) dCd, (b) dNi, and (c) dCu from KH-05-2 (along 160°W, 10°S–54°N); (d) dCd, (e) dNi, (f) dZn, and (g) dCu from GP02 (160°E–129°W, along 47°N); and (h) dCd, (i) dNi, (j) dZn, and (k) dCu from GP18 (along 165°E, 30°N–51°N). The white solid lines indicate potential density anomalies. NPIW: North Pacific Intermediate Water; EqPIW: Equatorial Pacific Intermediate Water; UCDW: Upper Circumpolar Deep Water; LCDW: Lower Circumpolar Deep Water; PDW: Pacific Deep Water.

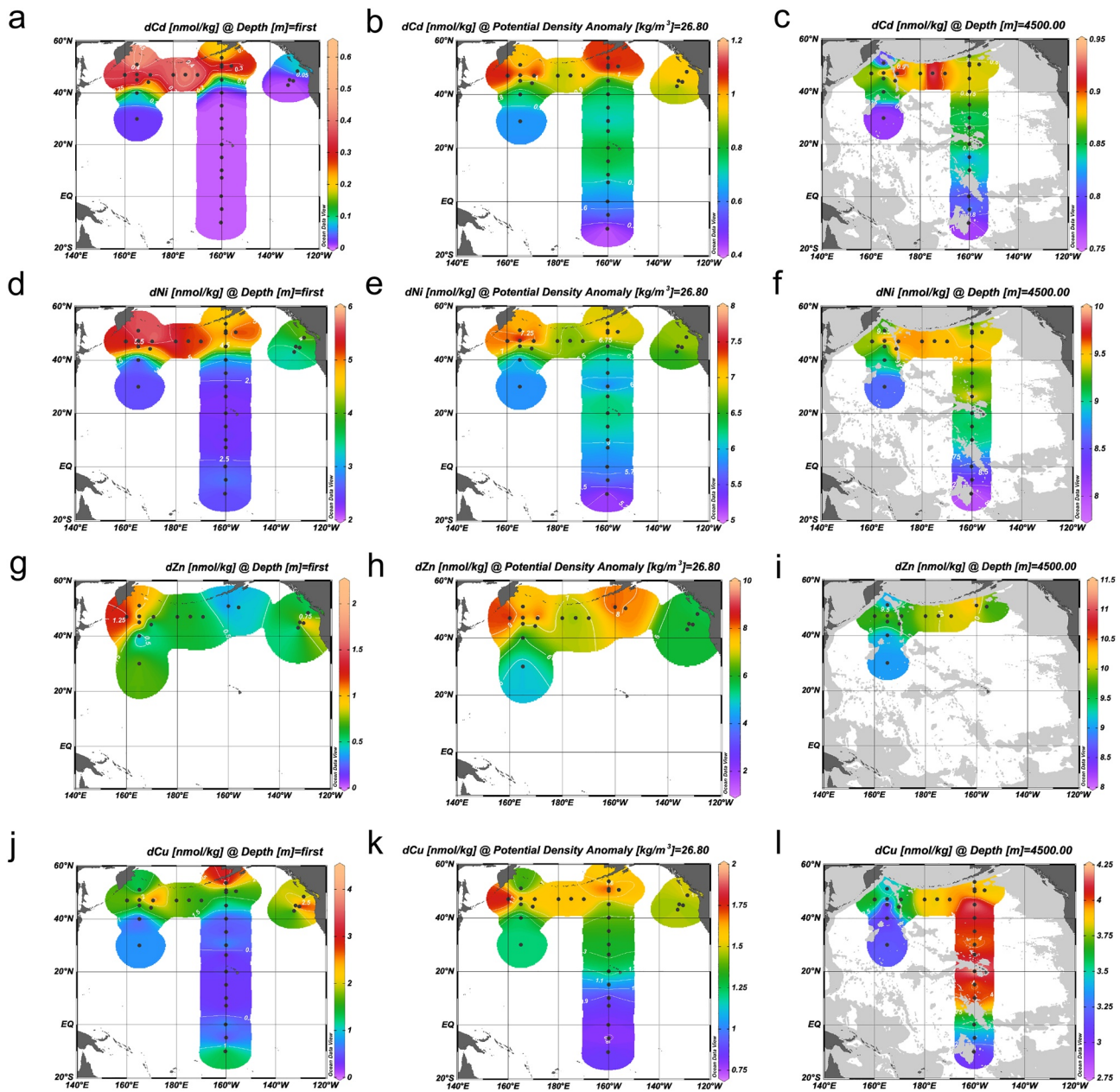


Figure 4. Horizontal distributions of (a)–(c) dCd, (d)–(f) dNi, (g)–(i) dZn, and (j)–(l) dCu on a surface of 10–20 m depth (left panels), $26.8 \sigma_{\theta}$, which is the center of NPIW (center panels), 4500 m depth where LCDW flows (right panels).

45°N (e.g., Figures S1a and S2a). Typically, the $l_p\text{Cd}$ was usually lower than DL (0.11 nmol/kg), which is consistent with previously reported low concentrations of particulate Cd ($0.05\text{--}38 \text{ pmol/kg}$) in the North Pacific (Bruland et al., 1994; Janssen et al., 2019). However, the $l_p\text{Cd}$ in this study was 0.16 nmol/kg in the surface layer at ST14, coinciding with the location of the highest Chl. *a* concentration. The $l_p\text{Cd}$ at TR15 was 0.24 nmol/kg at a 200 m depth, which is close to the Kamchatka Peninsula (KP).

The correlation coefficients between dNi and major nutrients were >0.91 for all data (Table S5). The dNi profiles exhibited the lowest concentrations ($2.3\text{--}5.9 \text{ nmol/kg}$) in surface water, a broad maximum of 10.5 nmol/kg at depths of 1500–3000 m with an exception of $8.8\text{--}9.7 \text{ nmol/kg}$ at the southernmost station (ST01), and a slight decrease above the bottom (Figures 3b, 3e, and 3i).

The broad maximum of dZn occurred at a depth of 1000–2000 m; this was deeper than that of dCd (Figures 3f and 3j). The correlation coefficients between dZn and major nutrients were >0.91 for all data, similar to dNi (Table S5).

The dCu increased linearly from surface to a depth of 3000 m (Figures 3c, 3g, and 3k). At stations to the south of 30°N and at depths of 3000–4000 m, dCu exhibited a maximum of 2.7–4.4 nmol/kg, which remained constant or decreased slightly below this depth. In contrast, at stations to the north of 40°N in the Northeast Pacific Basin and at the same depth, dCu was present at a lower concentration (2.4–3.1 nmol/kg), whereby the concentration generally increased toward the bottom. At a depth of 4500 m, the dCu had a uniformly high concentration from 10°N to 45°N (Figure 4l). The dM/tdM is 0.98 ± 0.23 for Cd ($n = 555$), 1.00 ± 0.04 for Ni ($n = 625$), 0.97 ± 0.14 for Zn ($n = 323$), and 0.86 ± 0.09 for Cu ($n = 617$). Thus, the lpM fraction (the difference between tdM and dM) is significant only for Cu. Among the four metals, only lpCu was observed for ~50% of all samples, indicating that suspended particulate matter contributed to the tdCu distribution. The sectional distribution of lpCu is shown in Figure S5; lpCu generally increased with depth, whereby the highest concentration of 1.37 nmol/kg was observed in abyssal seawater at TR13. The lpCu/tdCu ratio for all data was 0.18 ± 0.12 (ave \pm sd), which is as high as the lpM/tdM ratios (~0.2) observed for scavenged-type metals, such as Mn and Co (Zheng et al., 2019). Concentrations of the lpCd, lpNi, and lpZn are not discussed further as they were only detected in a few samples collected near the continents.

4. Discussion

4.1. dMs Versus PO₄

It is well-known that nutrient-type trace metals are required for phytoplankton growth or incorporated into phytoplankton for uncertain reasons and thus have strong correlation with major nutrients (Emerson & Hedges, 2008). However, relationship of dMs to major nutrients differs for different ocean basins. The dCd versus PO₄ plot for all data in this study exhibited a linear relationship:

$$\begin{aligned} \text{dCd} [\text{nmol/kg}] &= 0.360 \times \text{PO}_4 [\mu\text{mol/kg}] - 0.058 \\ r^2 &= 0.971, n = 605 \end{aligned} \quad (1)$$

The slope of 0.360 was in the range of the Cd/P ratio in phytoplankton (0.20–0.56 nmol/ μ mol) (Collier & Edmond, 1984; Ho et al., 2007, 2009). For more details, the plot shows a dependency on latitude (Figure 5a); dCd was not detected in 86% of the samples from the upper 100 m at stations to the south of 20°N. For waters at depths of 100–800 m at stations to the south of 20°N, the regression line had a slope of 0.358, which was near parallel to that defined by Equation 1. However, the intercept of -0.162 was much lower than that of -0.058 , resulting in a kink in the dCd versus PO₄ plot. In contrast, for samples excluding those from 0 to 800 m depths at stations to the south of 20°N, the regression line had a slope of 0.354 and an intercept of -0.034 . The comparable slopes of the three regression lines indicate that dCd and PO₄ are regenerated from sinking particles at a constant ratio throughout the North Pacific Ocean. The higher intercept at northern stations may be attributed to the continental source of dCd.

There was no linear relationship between dCu and PO₄ throughout the water column (Figure 5b). Instead, a kink was observed at a depth of 800 m. The overall slope was ~0.38 nmol/ μ mol in a depth range of 20–800 m, close to the Cu/P ratio in phytoplankton (0.37–1.1 nmol/ μ mol) (Bruland et al., 1991; Collier & Edmond, 1984; Ho et al., 2007; Kuss & Kremling, 1999). Data from stations to the south of 20°N were plotted below the regression line. Some samples from 0 to 20 m depth at stations to the north of 40°N had substantially high dCu. In deep waters, dCu increased independently of PO₄.

The relationship between dNi and PO₄ (Figure 5c) and between dZn and PO₄ (Figure 5d) appeared to be intermediate between those of dCd and PO₄ and between dCu and PO₄. There was a linear relationship between dNi and PO₄ only in the depth range of 0–500 m, and different regression lines were obtained for northern and southern stations (Figure 5c). The slopes of 1.37–1.50 nmol/ μ mol were close to the range of the Ni/P ratio in phytoplankton (0.22–1.4 nmol/ μ mol) (Bruland et al., 1991; Collier & Edmond, 1984; Ho et al., 2007; Kuss & Kremling, 1999). The intercept was significantly higher at stations to the north of 40°N, similar to that of dCd versus PO₄. In a depth range of 500–2000 m, dNi increased independently of PO₄.

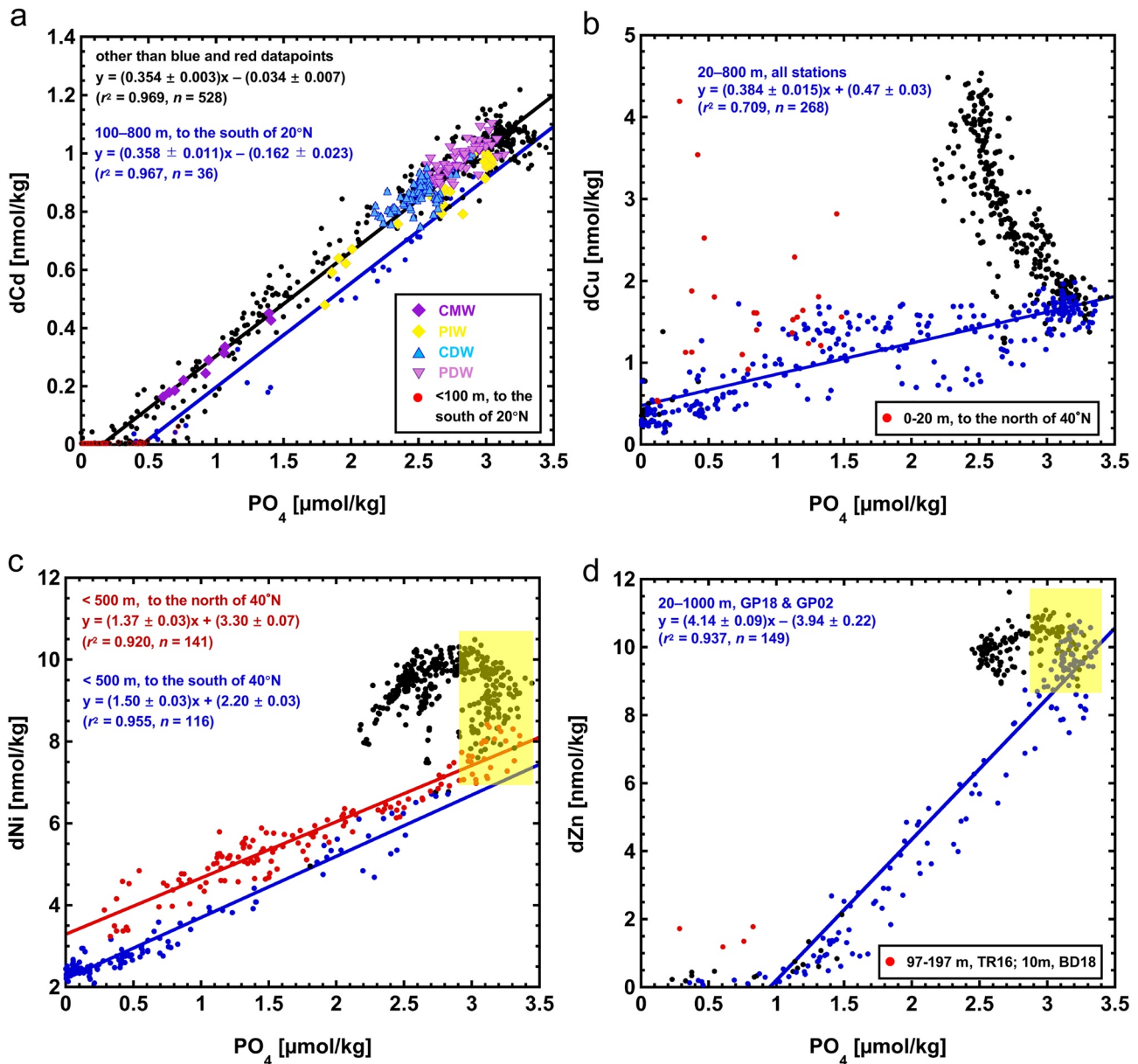


Figure 5. Plots of (a) dCd versus PO_4 , (b) dCu versus PO_4 , (c) dNi versus PO_4 , and (d) dZn versus PO_4 . The color lines indicate different regression lines. The yellow shadows indicate areas where dZn and dNi increase independently of PO_4 . Black dots indicate all data not included in colored classes. All the data used here are from this study.

(yellow shadow in Figure 5c). In deeper waters, dNi decreased concurrently with PO_4 in a manner similar to dCd. For dZn, the data were limited for stations to the north of $40^\circ N$. The dZn versus PO_4 plot showed a depletion of dZn in surface waters and a linear relationship from a depth of 20–1000 m (Figure 5d). However, substantially high concentrations of dZn were observed at depths of 99–197 and 10 m at TR11 and BD18, respectively. In the depth range of 1000–2000 m, dZn increased to its maximum independently of PO_4 , similar to dNi (yellow shadow in Figure 5d). Thus, dNi and dZn in intermediate-depth waters are independent of PO_4 . This means that processes other than regeneration from the organic matter, such as redissolution of minerals, are likely to play an important role in the distribution of these trace metals.

4.2. Input of dMs and Major Nutrients From the Continents

In surface waters, dCd and dNi were usually lower at stations to the south of 40°N compared with those located to the north of 40°N (Figures 4a and 4d). The major nutrients (Si(OH)₄, PO₄, and NO₃) showed similar distributions to dCd and dNi in surface waters (Figures S5a, S5d, and S5g), signifying the concurrent sources of these elements around the northern continents. However, surface concentrations of dCd, dNi and the major nutrients were low at ST14 compared with the surrounding stations. Chl. *a* concentration in surface water had the maximum at ST14 (Figure S4l). This suggests that the supply from the northern continents occurs in conjunction with the influence of phytoplankton uptake for dCd, dNi, and major nutrients.

The dZn in surface waters sharply decreased with distance from the western-most stations (TR16/BD07) near the Kuril–Kamchatka Trench (KKT) to stations in WSG (Figure 4g). This suggests a supply of dZn from the Sea of Okhotsk and uptake of dZn by phytoplankton. Surface concentrations of dCu were generally higher at northern stations, while extremely high concentrations occurred around JdFR and at ST14 near the Aleutian Islands (Figure 4j). Similarly, tdAl, tdMn, tdCo, and tdFe were present at high concentrations in surface waters at ST14, suggesting a concurrent supply of these elements from continental sources (Zheng & Sohrin, 2019; Zheng et al., 2019). In addition, some shallow water samples from the northern stations also contained substantially high concentrations of dCu and dZn, which were plotted above the regression lines in the dCu versus PO₄ and dZn versus PO₄ plots (Figures 5b and 5d). These results may be attributed to anthropogenic sources via aeolian transport (Liao et al., 2020).

At a surface of $\sigma_\theta = 26.8 \text{ kg/m}^3$, dCd, dNi, dZn, and dCu exhibited similar horizontal distributions; this is indicative of supply from the northern continents through NPIW (Figures 4b, 4e, 4h, and 4k). The supply from continental sources is in accordance with that reported in previous studies for Al, Mn, Fe, Co, and Cu (Elrod et al., 2004; Jacquot & Moffett, 2015; Johnson et al., 1997; Lam & Bishop, 2008; Nishioka & Obata, 2017; Zheng & Sohrin, 2019; Zheng et al., 2019), and for nutrients (Treguer et al., 1995).

4.3. Effects of Water Circulation and Biological Processes on the Distribution of dCd

Water circulation plays an important role in the distribution of dCd and affects the relationship between dCd and PO₄ (Xie et al., 2019; Yang et al., 2018; Zhang et al., 2019). In this study, the data points of dCd versus PO₄ converged on a single line at a slope of 0.354, excluding data from the upper 800 m at 10°S–20°N. This may be attributed to the mixing of central mode water (CMW), Pacific Intermediate Waters (PIW that includes NPIW and EqPIW), CDW, and PDW (Figure 5a).

The fractionation factor (*FF*) was defined to investigate the preferential uptake of dCd over PO₄ using Equation 2 (Elderfield & Rickaby, 2000; Quay et al., 2015):

$$FF(dCd) = \left(\text{Cd:PO}_{4, \text{particles}} \right) / \left(\text{dCd/PO}_{4, \text{seawater}} \right) \quad (2)$$

where the Cd:PO_{4, particles} was estimated from the slope of the dCd versus PO₄ plot in the nutricline (typically 50–800 m in depth), as this slope is representative of the regeneration ratio of biogenic particles (Lane et al., 2009). The dCd/PO_{4, seawater} was estimated from the average of spot concentration ratios from the surface mixed layer (typically 0–50 m in depth). The *FF*(dCd) in this study varied from ~0.7 at northern stations to >10 at stations to the south of 10°N and around JdFR. It averaged to 9.2 ± 13.1 (Figure 6a), which is much higher and more scattered than the reported value of 1.8 ± 1.0 in the North Pacific (Quay et al., 2015). The *FF* was 1.4 ± 0.7 for stations (BD7–BD16 from GP02, TR13–TR16 from GP18, and ST12–ST14 from KH-05-2) located in NPSAG, a HNLC region, and the average PO₄ concentration in the surface mixed layer was $1.0 \pm 0.3 \text{ } \mu\text{mol/kg}$. In contrast, the *FF* was 17 ± 15 with a maximum of 45 for stations outside the NPSAG, where the average PO₄ concentration in the surface mixed layer was $0.2 \pm 0.2 \text{ } \mu\text{mol/kg}$. These results indicate that the preferential uptake of dCd is insignificant in the NPSAG. This is inconsistent with previous observations (Cullen, 2006; Quay et al., 2015) and calculation (Quay et al., 2015) in other HNLC areas. This may be attributed to the lower surface ratio of dCd/PO₄ at the southern stations in this study excluding ST07 near the Hawaiian Islands. (Figure S4j) and/or supply from continent to the northern stations.

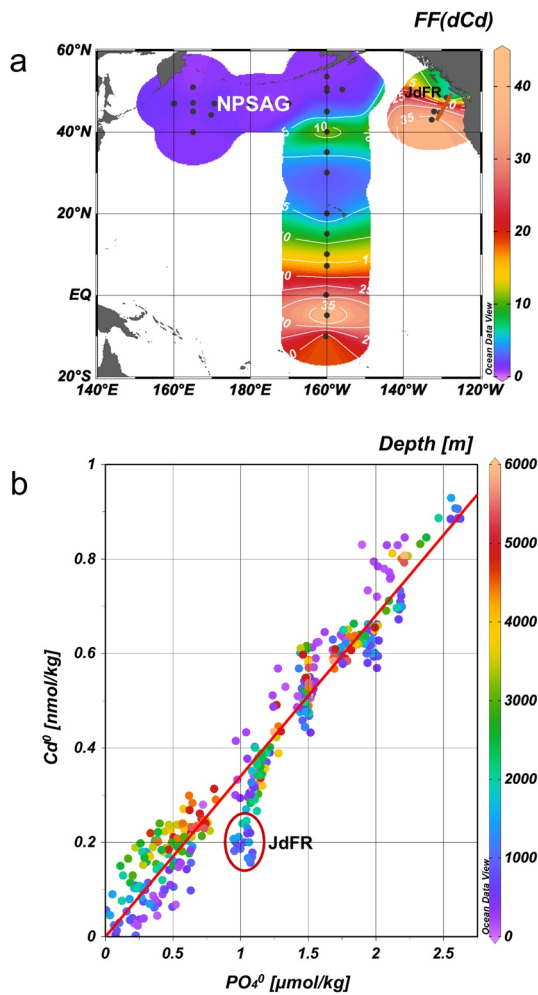


Figure 6. (a) Horizontal distribution of the fractionation factor of dCd (FF), (b) preformed Cd (dCd^0) versus preformed phosphate (PO_4^0) plot. The point color shows depth. The red circle indicates data obtained from the JdFR.

Preformed nutrient concentrations have been used as tracers for water masses due to their conservative nature (Sarmiento & Gruber, 2006). Redfield et al. (1963) established the respiratory equation of the average phytoplankton, determining that the ratio of dissolved PO_4 to O_2 was 1:138. As such, preformed phosphate (PO_4^0) was defined as per Equation 3 (Emerson & Hedges, 2008; Kudo et al., 1996):

$$PO_4^0 [\mu\text{mol/kg}] = PO_4 - AOU/138 \quad (3)$$

We used the slope of PO_4 versus AOU (apparent oxygen utilization) in the upper 800 m instead of 138. The data in surface waters with AOU < 0 were excluded from the calculation. Assuming that the Redfield ratio may be extended to dCd (Kudo et al., 1996), the preformed dCd (dCd^0) was defined as:

$$dCd^0 [\text{nmol/kg}] = dCd - AOU \times (a \times b) \quad (4)$$

where data from the upper 800 m was used to determine a and b , which denote the slopes for the plots of dCd versus PO_4 and PO_4 versus AOU, respectively. The dCd^0 data from the upper 800 m waters were generally less than zero. Data of $dCd^0 < 0$ were excluded in the discussion. The plots of dCd^0 versus PO_4^0 had a strong linear relationship with an intercept of zero (Figure 6b).

$$dCd^0 [\text{nmol/kg}] = 0.341 \times PO_4^0 - 0.000 \quad (5)$$

$$r^2 = 0.931, n = 379$$

The zero intercept indicates that the remineralization ratio of $dCd^0:PO_4^0$ was constant among water masses, while the slope of 0.341 was equal to the observed spot concentration ratio of dCd/ PO_4 in deep waters. The linearity of Equation 5 also supports the dominant effect of water circulation and biological processes on dCd distribution. Plots that deviate from the regression line are marked by a red circle in Figure 6b, representing data from JdFR. This is likely due to the removal of CdS near the hydrothermal vents of the JdFR (Zheng et al., 2017).

These findings discussed above suggest that the disappearance of the kink in relationship between dCd and PO_4 at stations to the north of 20°N, was caused by a combination of the supply of dCd from the northern continents and the nonpreferential uptake of dCd by phytoplankton in the NPSAG.

4.4. Effects of Water Circulation, Scavenging, and Remineralization on the Distribution of Cu, Ni, and Zn

4.4.1. Water Circulation: dMs Versus $Si(OH)_4$

It has been proposed that the Southern Ocean is an important region influencing the global intermediate and deep water distributions of dZn and $Si(OH)_4$ (Ellwood, 2008; Vance et al., 2017; Wyatt et al., 2014). However, the impact of the mechanisms arising from the Southern Ocean on the relationship between trace metals and major nutrients in the North Pacific is unclear. The data from this study demonstrate that this hypothesis alone cannot fully explain the relationship in the North Pacific as discussed below.

Studies on the relationship between dCu and $Si(OH)_4$ in the ocean have commenced since the 1980s (Monteiro & Orren, 1985; Roshan & Wu, 2015b; Saager et al., 1992), as shown in Figure 1c. Table 2 presents the regression lines of waters in depth ranges of 0–1500 m and 1500 m–bottom from different ocean basins. The

Table 2
Regression Lines for Cu vs. Si(OH)₄ in Waters of 0–1500 m and 1500 m–Bottom

	North Atlantic Ocean		South Atlantic Ocean		Southern Ocean		Indian Ocean		South Pacific Ocean		North Pacific Ocean	
0–1500 m												
	ave	sd	ave	sd	ave	sd	ave	sd	ave	sd	ave	sd
Slope	0.0129	± 0.0011	0.0144	± 0.0028	0.0121	± 0.0010	0.0117	± 0.001	0.0136	± 0.000	0.0072	± 0.0002
Intercept	0.911	± 0.012	0.779	± 0.076	0.743	± 0.078	0.770	± 0.053	0.506	± 0.014	0.786	± 0.030
<i>r</i> ²	0.171		0.255		0.701		0.562		0.921		0.850	
<i>n</i>	670		80		70		69		171		160	
1500 m–bottom												
	ave	sd	ave	sd	ave	sd	ave	sd	ave	sd	ave	sd
Slope	0.037	± 0.001	0.019	± 0.001	0.026	± 0.007	0.049	± 0.007	0.043	± 0.004	-0.013	± 0.004
Intercept	0.780	± 0.036	0.763	± 0.057	-0.625	± 0.800	-2.206	± 0.793	-2.218	± 0.587	5.311	± 0.617
<i>r</i> ²	0.695		0.836		0.307		0.596		0.274		0.056	
<i>n</i>	425		157		37		37		248		201	

dCu in a depth range of 0–1500 m in the Atlantic Ocean was weakly correlated with Si(OH)₄ ($r^2 < 0.26$), while dCu in the Southern and Pacific Oceans was strongly correlated with Si(OH)₄ ($r^2 > 0.70$). In contrast, correlations in a depth range of 1500 m–bottom encompassed entirely different trends (Figure 1c): a strong correlation ($r^2 > 0.69$) in the Atlantic Ocean, and a weak correlation ($r^2 = 0.31$) in the Southern Ocean. There was no significant correlation for waters >1500 m in depth in the North Pacific Ocean (Figures 1c and Table 2). The dCu versus Si(OH)₄ plot in this study is shown in Figure S6a. The data in a depth range of 20–1500 m contained two regression lines; the line for the northern stations had a lower slope and higher intercept than its counterpart for the southern stations. The dCu in the deep North Pacific Ocean increased independently with Si(OH)₄ (Figure S6a). This phenomenon is largely due to the redissolution of scavenged dCu from particles and sediments (Takano et al., 2014). The stagnant deep-water circulation in the North Pacific Ocean enhanced the accumulation of dCu compared with other oceans.

The relationship between dZn and Si(OH)₄ in this study exhibited an upward curve with a kink at 84 μmol/kg of Si(OH)₄ (Figure S6b). Kim et al. (2017, 2015) observed the same trend and attributed this kink to the supply of intermediate waters with a high dZn/Si(OH)₄ ratio. Figure 1b shows that the data from deep waters (>1500 m in depth) exhibited entirely different trends between the Southern and North Pacific Oceans. In the dNi versus Si(OH)₄ plot of this study, a convex trend was observed at stations to the south of 40°N (Figure S6c), indicating the effect of EqPIW and UCDW with a high dNi/Si(OH)₄ ratio (Table S6). In contrast, data for stations to the north of 40°N exhibited linearity throughout the water column. There was no linear relationship between dCd and Si(OH)₄ (Figure S6d). These results indicate that water circulation or the mechanism in the Southern Ocean cannot fully explain the relationship between dMs and Si(OH)₄, particularly for the deep waters in the North Pacific Ocean.

4.4.2. Scavenging and Remineralization: dMs/PO₄

Cu, Ni, and Zn are widely utilized as cofactors of enzymes (Twining & Baines, 2013), and are incorporated into the soft tissue of organisms in a similar manner to Cd. Ellwood and Hunter (2000) have demonstrated that only a small percentage of Zn is incorporated in diatom frustules, which may also apply to Ni and Cu.

NO₃ and PO₄ are mainly influenced by water circulation and biological processes, resulting in a strong relationship with each other (Figure S3d, Table S5). In waters deeper than 800 m, the dCd/PO₄ ratio decreased by $4 \pm 3\%$ when the AOU increased from 150 to 300 μmol/kg ($p = 8.5 \times 10^{-6}$, Figure 7a). In contrast, dNi/PO₄, dZn/PO₄, and dCu/PO₄ decreased by $21 \pm 3\%$, $21 \pm 4\%$, and $69 \pm 7\%$, respectively (Figures 7b–7d). The decrease in NO₃/PO₄ was $6 \pm 3\%$, which is comparable to that of dCd/PO₄. These results indicate that scavenging, as an alternative sink, is important for Cu, Ni, and Zn. Otherwise, their ratios would not change with AOU.

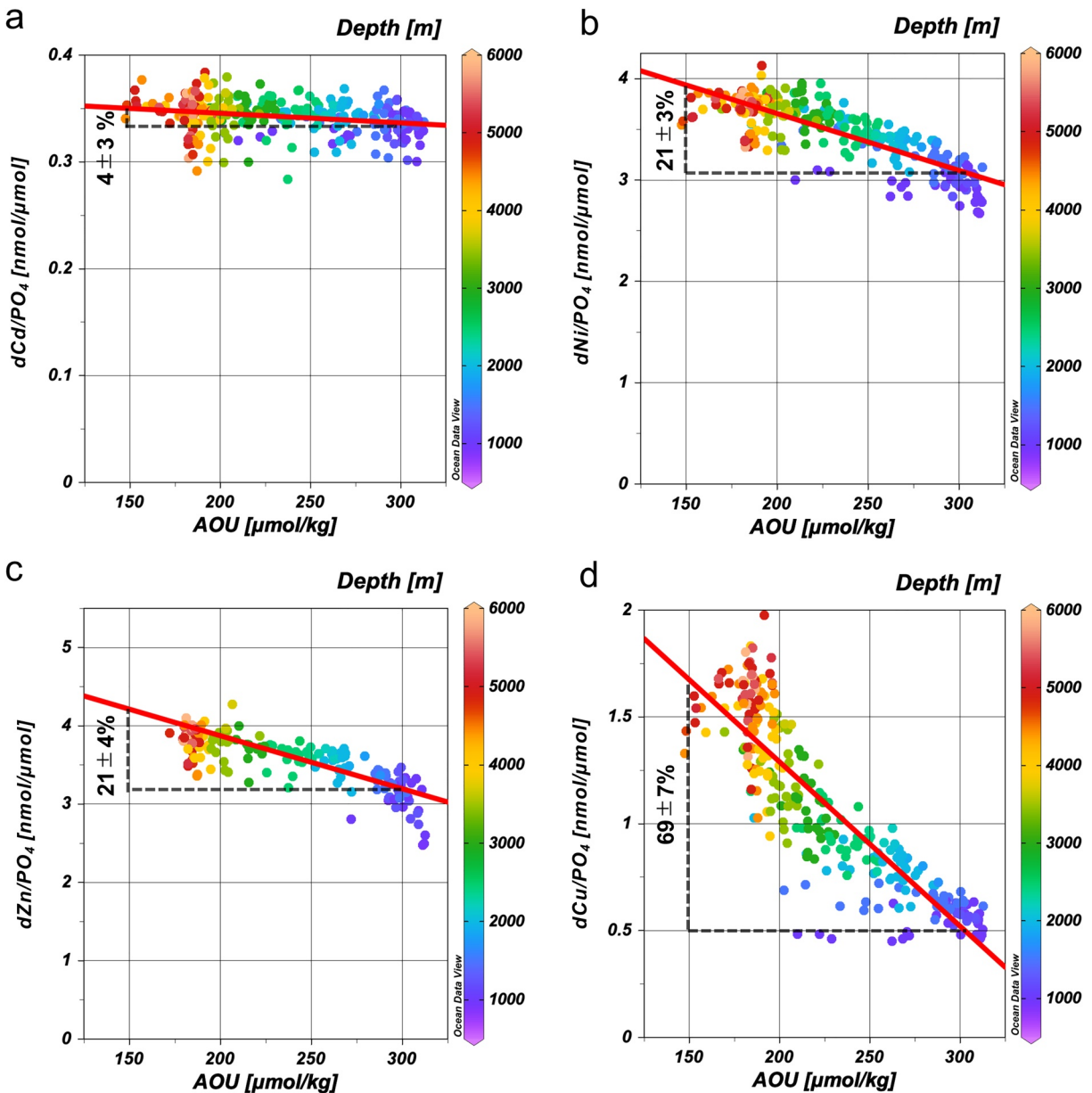


Figure 7. Plots of dMs/PO₄ ratios versus AOU at depths > 800 m: (a) dCd/PO₄ versus AOU, (b) dNi/PO₄ versus AOU, (c) dZn/PO₄ versus AOU, and (d) dCu/PO₄ versus AOU. The point color indicates depth.

Figure 8 presents the vertical profiles of the dMs/PO₄ spot concentration ratio, where the metal to phosphorus ratio (M/P) range in phytoplankton is depicted using a gray shadow (Bruland et al., 1991; Collier & Edmond, 1984; Ho et al., 2007; Kuss & Kremling, 1999). Almost all dCd/PO₄ data are within the range of phytoplankton, indicating that the Redfield ratio concept is also applicable to Cd. However, the plots for dNi, dCu, and dZn were largely outside the phytoplankton range. Table S6 lists the dMs/PO₄ ratios for each water mass. In the upper 200 m, the dCd/PO₄ ratio was generally lower than the Cd/P ratio in phytoplankton at stations to the south of 40°N (Figure 8a). Given that dCd had a residence time ~10 times shorter than that of PO₄ in the surface mixed layer (Table S7), it was possible that surface dCd/PO₄ becomes much lower than that in phytoplankton. The dCd/PO₄ ratio was 0.34 ± 0.02 nmol/μmol ($n = 296$) at a depth >800 m, consistent with previously published data (Quay et al., 2015). Figure S7 shows the sectional distribution of dM/PO₄ in the waters of the upper 1000 m from the KH-05-2 cruise. The dCd/PO₄ ratio varied significantly and was substantially lower in the upper waters at stations south of 20°N; this again emphasizes the

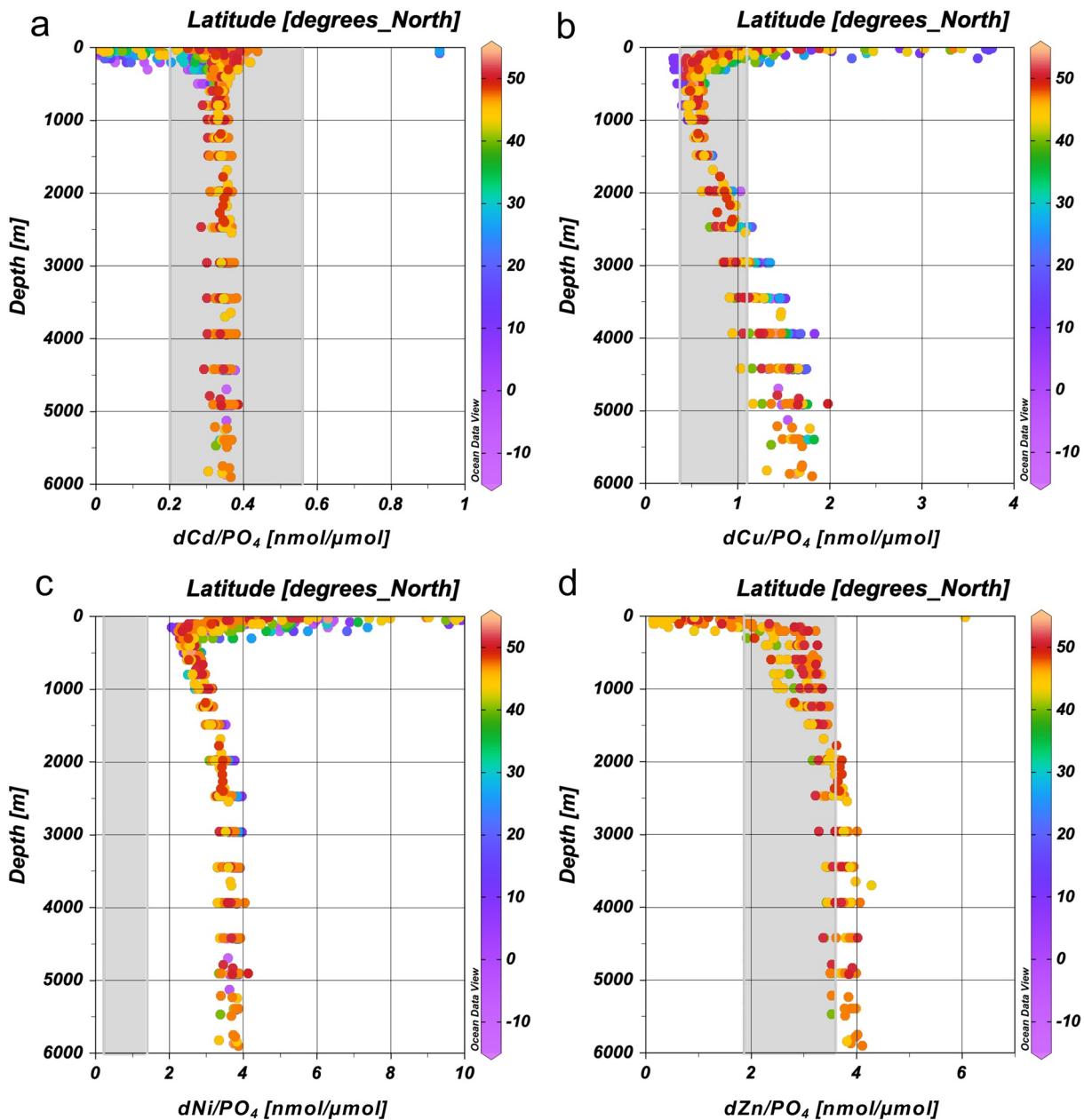


Figure 8. Vertical profiles of (a) dCd/PO₄, (b) dNi/PO₄, (c) dZn/PO₄, and (d) dCu/PO₄. The gray shadows mark the range of the Ms/PO₄ ratio in phytoplankton (Bruland et al., 1991; Collier & Edmond, 1984; Ho et al., 2007; Kuss & Kremling, 1999).

preferential uptake of dCd. The dCd/PO₄ ratio reached a maximum of 0.93 nmol/μmol in surface waters around 20–30°N, where PO₄ is depleted and dCd is likely to be supplied from the Hawaiian Islands. An additional high Cd/PO₄ ratio was identified near the northern continental shelf and spread to ~20°N along 26.8σ_θ in the presence of intermediate waters (Figure S4k); this distribution was similar to that of dCo (Zheng et al., 2019).

Despite the similar residence times of dCu and PO₄ in the surface mixed layer (Table S7), the dCu/PO₄ ratio was extremely high, reaching a maximum of 82 nmol/μmol in surface waters around 20–30°N, similar to dCd/PO₄ (Figure S7b). The dCu/PO₄ ratio decreased sharply in subsurface waters to a minimum of 0.30 nmol/μmol (Figure 8b) at depths from 150 to 800 m, signifying regeneration of PO₄ and the scavenging of dCu. Then, the dCu/PO₄ ratio increased toward deeper waters, while many data points were outside

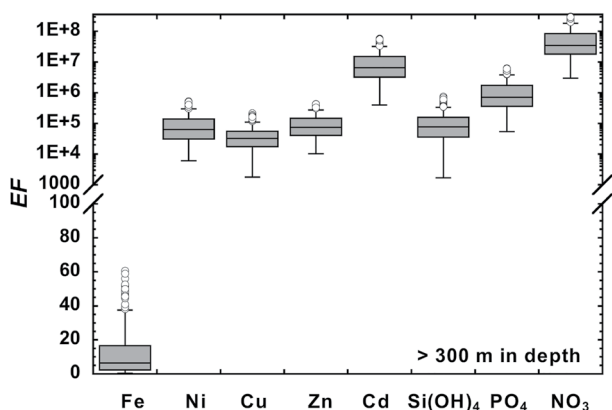


Figure 9. Box plots of EF for dFe , dCu , dNi , dZn , dCd , and major nutrients at depths > 300 m in this study. The middle line of the box represents the median; the top and bottom lines of the box represent the upper and lower quartiles, respectively; and circles represent potential outliers.

ratio was 3.1 ± 0.3 nmol/ μ mol at a depth range of 600–1500 m, which is significantly lower than that of 3.8 ± 0.2 nmol/ μ mol below 3000 m. The low ratio in the intermediate depth may be attributed to the scavenging of dZn (Little et al., 2013; Weber et al., 2018), and/or water mass mixing (Kim et al., 2017). In addition, the ratio in deep water exceeds the range of the Zn/P ratio in phytoplankton, suggesting that additional dZn was supplied via the redissolution from sinking particles and bottom sediments.

The abundance of $lpCu$ in deep waters was also a result of scavenging (Figure S5). The $lpCu/tdCu$ ratio was 0.12 ± 0.05 ($n = 227$) in deep waters (>1500 m) of the North Pacific Ocean, exhibiting a smaller deviation in deep waters than in the upper waters. Moreover, the $lpCu/tdCu$ ratio was comparable to that of the scavenged-type Mn and Co (~ 0.2) (Zheng et al., 2019). Cu was the only element among the four nutrient-type metals whose lp species were broadly detected in the North Pacific Ocean. The high percentage of $lpCu$ may be attributable to the adsorption of dCu onto particles, largely governed by surface complexation (Li, 1981). The stability of the surface complexes exhibits a linear relationship with the first hydrolysis constant for metal ions. As the four metal ions in this study form divalent cations and Cu^{2+} has the highest first hydrolysis constant (Li, 1981), Cu exhibited the highest lpM/tdM ratio and the strongest scavenging. In contrast, Cd^{2+} had the lowest first hydrolysis constant, resulting in reduced scavenging activity.

The scavenging of Ni has not yet been widely accepted. However, the residence time of dMs in oceans around the world has been estimated to be 5,000 years for Cu (Boyle et al., 1977), 10,000–30,000 years for Ni (Cameron & Vance, 2014; Sclater et al., 1976), 18,000 years for Zn (Bewers & Yeats, 1977), and 50,000 years for Cd (Boyle et al., 1976; Bruland, 1980) (Table S7). In addition, the scavenging residence time was estimated to be 385 years for Cu, 15,850 years for Ni, and 177,800 years for Cd (Balistrieri et al., 1981). In the near-ridge environment, sedimentary Ni concentrations increased because of the scavenging of dNi from seawater by Mn and Fe (oxyhydr)oxides (Costa et al., 2018; Dunk & Mills, 2006; Metz et al., 1988). As such, it is postulated that scavenging is an important factor for Ni, Cu and Zn in the North Pacific Ocean.

4.5. Systematics in Enrichment Factor

The enrichment factor (EF) of dMs in seawater was proposed in our previous studies to clarify the sources and sinks of dMs (Zheng & Sohrin, 2019; Zheng et al., 2019). It is expressed using

$$EF(dM) = \left(\frac{dM/dAl}{(M/Al)_{\text{upper crust}}} \right)_{\text{seawater}} \quad (6)$$

where $(M/Al)_{\text{upper crust}}$ represents the mole ratio in the upper crust (Rudnick & Gao, 2005). Figure 9 presents the box plots of EF for dFe , dissolved nutrient-type metals, and major nutrients at depths >300 m. The

the range of the Cu/P ratio in phytoplankton. The high dCu/PO_4 ratio was due to the selective accumulation of dCu in deep waters through water circulation and redissolution from sinking particles and bottom sediments.

Similar to dCu/PO_4 and dCd/PO_4 , the dNi/PO_4 ratio in surface waters was extremely high at stations around 20–30°N (Figure S7c). It then decreased to the subsurface minima of 2 nmol/ μ mol at 200 m and slightly increased to a depth of 3000 m (Figure 8c). All data of the dNi/PO_4 ratios were outside the range of the Ni/P ratio in phytoplankton. As the residence time of dNi is similar to that of PO_4 in the ocean (Table S7), these higher ratios are considered a result of excess dNi throughout the North Pacific Ocean.

For stations at GP18 and GP02, the dZn/PO_4 ratio in surface waters was low, between 0.15 and 1.2 nmol/ μ mol, with the exception of 6.0 nmol/ μ mol at BD18 (Figure 8d). These results suggest that the preferential uptake of dZn by phytoplankton is ubiquitous in the subarctic North Pacific Ocean. The dZn/PO_4 ratio increased with depth, while the dCd/PO_4 ratio was constant below 1000 m. This may suggest that reversible scavenging has a greater influence on dZn than dCd . For details, the dZn/PO_4

median EF was 7.1 for dFe , 3.2×10^4 for dCu , 6.3×10^4 for dNi , 7.4×10^4 for dZn , 6.6×10^6 for dCd , 7.7×10^4 for $Si(OH)_4$, 7.1×10^5 for PO_4 , and 3.5×10^7 for NO_3 . The dCd exhibited the highest EF among the four nutrient-type metals; this was one order of magnitude lower than that of NO_3 , reflecting the lowest influence of scavenging on dCd . Furthermore, $EF(dFe)$ was the lowest among the five metals, as dFe was demonstrated to be strongly affected by scavenging in the Pacific Ocean via field studies (Bruland et al., 1994; John et al., 2018; Landing & Bruland, 1987; Zheng & Sohrin, 2019) and model studies (Tagliabue et al., 2019). $EF(dCu)$, $EF(dNi)$, and $EF(dZn)$ were of the same order of magnitude, which was two orders of magnitude lower than $EF(dCd)$ and three orders of magnitude higher than $EF(dFe)$. These results suggest that dCu , dNi , and dZn have moderate interactions with particles.

The solubility of Ms may affect the $EF(dMs)$. It has been observed that the solubility of the four metals and Al from aerosols deposited on the sea surface differ significantly depending on various factors, such as source of the aerosols (Chester et al., 1993) and distance from the continent (Chester et al., 1993; Hsu et al., 2010; Mahowald et al., 2018). However, the average solubility of the four metals and Al from East China Sea aerosols was within a factor of 20 (Hsu et al., 2010). Thus, solubility is not considered to significantly influence the trend shown in Figure 9.

This study demonstrates that $EF(dMs)$ may be a promising parameter that can be used to determine whether an element is effectively scavenged through the water column, particularly below the surface mixed layer. As $EF(dCu)$, $EF(dNi)$, and $EF(dZn)$ are comparable, we infer that dCu , dZn , and dNi are affected by scavenging processes.

5. Conclusions

This study used samples collected during the GEOTRACES Japan cruises KH-05-2, KH-11-7 (GP18), and KH-12-4 (GP02) in the North Pacific Ocean to determine sectional dissolved Cd , Ni , Zn , Cu , and labile particulate Cu distributions in the North Pacific Ocean. These data indicate that dCd is influenced by biological processes and water circulation. Although this was also the case for dNi , dZn , and dCu , these metals were affected by scavenging. The effects from scavenging of the four metals were detected due to the internal formation of PDW in the North Pacific Ocean and its long residence time. Each metal had a unique relationship with the major nutrients, $Si(OH)_4$ and PO_4 , and there were strong differences in the relationships between dMs and nutrients from those reported in other oceans. The stoichiometry among dMs and major nutrients, namely $FF(dCd)$, preformed dCd , dMs/PO_4 concentration ratio, and $EF(dMs)$, can enhance the current understanding of the effect of internal cycles, scavenging, and redissolution on the distribution of metals. As such, we conclude that, among the four metals, Cu was the most affected by scavenging, while Cd was the least affected, and scavenging played a significant role on Ni and Zn distributions.

Data Availability Statement

The raw data are archived at PANGAEA (<https://doi.org/10.1594/PANGAEA.932280>).

References

- Archer, C., Vance, D., Milne, A., & Lohan, M. C. (2020). The oceanic biogeochemistry of nickel and its isotopes: New data from the South Atlantic and the Southern Ocean biogeochemical divide. *Earth and Planetary Science Letters*, 535, 116118. <https://doi.org/10.1016/j.epsl.2020.116118>
- Baars, O., Abouchami, W., Galer, S. J. G., Boye, M., & Croot, P. L. (2014). Dissolved cadmium in the Southern Ocean: Distribution, speciation, and relation to phosphate. *Limnology & Oceanography*, 59(2), 385–399. <https://doi.org/10.4319/lo.2014.59.2.0385>
- Balistrieri, L., Brewer, P. G., & Murray, J. W. (1981). Scavenging residence times of trace metals and surface chemistry of sinking particles in the deep ocean. *Deep-Sea Research A*, 28(2), 101–121. [https://doi.org/10.1016/0198-0149\(81\)90085-6](https://doi.org/10.1016/0198-0149(81)90085-6)
- Bewers, J. M., & Yeats, P. A. (1977). Oceanic residence times of trace metals. *Nature*, 268(5621), 595–598. <https://doi.org/10.1038/268595a0>
- Bostock, H. C., Opydyke, B. N., & Williams, M. J. M. (2010). Characterizing the intermediate depth waters of the Pacific Ocean using $\delta^{13}C$ and other geochemical tracers. *Deep-Sea Research I*, 57(7), 847–859. <https://doi.org/10.1016/j.dsr.2010.04.005>
- Boyle, E. A. (1988). Cadmium: Chemical tracer of deepwater paleoceanography. *Paleoceanography*, 3(4), 471–489. <https://doi.org/10.1029/pa003i004p00471>
- Boyle, E. A., Huested, S. S., & Jones, S. P. (1981). On the distribution of copper, nickel, and cadmium in the surface waters of the North Atlantic and North Pacific Ocean. *Journal of Geophysical Research*, 86(C9), 8048–8066. <https://doi.org/10.1029/jc086ic09p08048>

Acknowledgments

The authors thank the crew, technicians, students, and scientists onboard the KH-05-2, KH-11-7, and KH-12-4 cruises for their assistance with sampling and analysis of routine parameters. The authors also thank graduate student Wataru Konagaya for his assistance in the determination of trace metals in some samples from the KH-11-7 and KH-12-4 cruises. The authors are grateful to Editor Sara Mikaloff Fletcher, Associate Editor Benjamin S. Twining, and the two anonymous reviewers for their comments and suggestions. This study was supported by KAKENHI grants (Grant Nos 16204046, 21350042, 24241004, 15H01727, and 19H01148) from the Japan Society for the Promotion of Science, by Mitsumasa Ito Memorial Research Grants (H30-R3 and H31-R1) from the Research Institute for Oceanography Foundation, by the Sasakawa Scientific Research Grant (2019–3036) from the Japan Science Society, by the International Collaborative Research Program (2019–47) from the Institute for Chemical Research, Kyoto University, and by the Future Development Funding Program of Kyoto University Research Coordination Alliance. The authors thank Editage (www.editage.com) for English language editing.

- Boyle, E. A., Sclater, F., & Edmond, J. M. (1976). On the marine geochemistry of cadmium. *Nature*, 263(5572), 42–44. <https://doi.org/10.1038/263042a0>
- Boyle, E. A., Sclater, F., & Edmond, J. M. (1977). The distribution of dissolved copper in the Pacific. *Earth and Planetary Science Letters*, 37(1), 38–54. [https://doi.org/10.1016/0012-821x\(77\)90144-3](https://doi.org/10.1016/0012-821x(77)90144-3)
- Broecker, W. S., & Peng, T.-H. (1982). *Tracers in the sea*. Eldigio Press.
- Bruland, K. W. (1980). Oceanographic distributions of cadmium, zinc, nickel, and copper in the North Pacific. *Earth and Planetary Science Letters*, 47(2), 176–198. [https://doi.org/10.1016/0012-821x\(80\)90035-7](https://doi.org/10.1016/0012-821x(80)90035-7)
- Bruland, K. W., Donat, J. R., & Hutchins, D. A. (1991). Interactive influences of bioactive trace metals on biological production in oceanic waters. *Limnology & Oceanography*, 36(8), 1555–1577. <https://doi.org/10.4319/lo.1991.36.8.1555>
- Bruland, K. W., Orians, K. J., & Cowen, J. P. (1994). Reactive trace metals in the stratified central North Pacific. *Geochimica et Cosmochimica Acta*, 58(15), 3171–3182. [https://doi.org/10.1016/0016-7037\(94\)90044-2](https://doi.org/10.1016/0016-7037(94)90044-2)
- Buck, K. N., & Bruland, K. W. (2005). Copper speciation in San Francisco Bay: A novel approach using multiple analytical windows. *Marine Chemistry*, 96(1), 185–198. <https://doi.org/10.1016/j.marchem.2005.01.001>
- Cameron, V., & Vance, D. (2014). Heavy nickel isotope compositions in rivers and the oceans. *Geochimica et Cosmochimica Acta*, 128(0), 195–211. <https://doi.org/10.1016/j.gca.2013.12.007>
- Chester, R., Murphy, K. J. T., Lin, F. J., Berry, A. S., Bradshaw, G. A., & Corcoran, P. A. (1993). Factors controlling the solubilities of trace metals from non-remote aerosols deposited to the sea surface by the ‘dry’ deposition mode. *Marine Chemistry*, 42(2), 107–126. [https://doi.org/10.1016/0304-4203\(93\)90241-f](https://doi.org/10.1016/0304-4203(93)90241-f)
- Collier, R., & Edmond, J. (1984). The trace element geochemistry of marine biogenic particulate matter. *Progress in Oceanography*, 13(2), 113–199. [https://doi.org/10.1016/0079-6611\(84\)90008-9](https://doi.org/10.1016/0079-6611(84)90008-9)
- Conway, T. M., & John, S. G. (2015). Biogeochemical cycling of cadmium isotopes along a high-resolution section through the North Atlantic Ocean. *Geochimica et Cosmochimica Acta*, 148(0), 269–283. <https://doi.org/10.1016/j.gca.2014.09.032>
- Costa, K. M., Anderson, R. F., McManus, J. F., Winckler, G., Middleton, J. L., & Langmuir, C. H. (2018). Trace element (Mn, Zn, Ni, V) and authigenic uranium (aU) geochemistry reveal sedimentary redox history on the Juan de Fuca Ridge, North Pacific Ocean. *Geochimica et Cosmochimica Acta*, 236, 79–98. <https://doi.org/10.1016/j.gca.2018.02.016>
- Croghan, C., & Egeghy, P. P. (2003). Methods of dealing with values below the limit of detection using SAS. Southern SAS User Group, 22, 24.
- Cullen, J. T. (2006). On the nonlinear relationship between dissolved cadmium and phosphate in the modern global ocean: Could chronic iron limitation of phytoplankton growth cause the kink? *Limnology & Oceanography*, 51(3), 1369–1380. <https://doi.org/10.4319/lo.2006.51.3.1369>
- Danielsson, L.-G., Magnusson, B., & Westerlund, S. (1985). Cadmium, copper, iron, nickel and zinc in the north-east Atlantic Ocean. *Marine Chemistry*, 17(1), 23–41. [https://doi.org/10.1016/0304-4203\(85\)90034-9](https://doi.org/10.1016/0304-4203(85)90034-9)
- De Baar, H. J. W., Saager, P. M., Nolting, R. F., & van der Meer, J. (1994). Cadmium versus phosphate in the world ocean. *Marine Chemistry*, 46(3), 261–281. [https://doi.org/10.1016/0304-4203\(94\)90082-5](https://doi.org/10.1016/0304-4203(94)90082-5)
- Dunk, R. M., & Mills, R. A. (2006). The impact of oxic alteration on plume-derived transition metals in ridge flank sediments from the East Pacific Rise. *Marine Geology*, 229(3), 133–157. <https://doi.org/10.1016/j.margeo.2006.03.007>
- Elderfield, H. (2003). (Ed.), *The oceans and marine geochemistry*. Elsevier-Pergamon.
- Elderfield, H., & Rickaby, R. E. M. (2000). Oceanic Cd/P ratio and nutrient utilization in the glacial Southern Ocean. *Nature*, 405(6784), 305–310. <https://doi.org/10.1038/35012507>
- Ellwood, M. J. (2008). Wintertime trace metal (Zn, Cu, Ni, Cd, Pb and Co) and nutrient distributions in the Subantarctic Zone between 40–52°S; 155–160°E. *Marine Chemistry*, 112(1–2), 107–117. <https://doi.org/10.1016/j.marchem.2008.07.008>
- Ellwood, M. J., & Hunter, K. A. (2000). The incorporation of zinc and iron into the frustule of the marine diatom *Thalassiosira pseudonana*. *Limnology & Oceanography*, 45(7), 1517–1524. <https://doi.org/10.4319/lo.2000.45.7.1517>
- Elrod, V. A., Berelson, W. M., Coale, K. H., & Johnson, K. S. (2004). The flux of iron from continental shelf sediments: A missing source for global budgets. *Geophysical Research Letters*, 31, L12307. <https://doi.org/10.1029/2004gl020216>
- Emerson, S. R., & Hedges, J. I. (2008). *Chemical Oceanography and the marine carbon cycle* (p. 222). Cambridge University Press
- Fischer, K., Dymond, J., Lyle, M., Soutar, A., & Rau, S. (1986). The benthic cycle of copper: Evidence from sediment trap experiments in the eastern tropical North Pacific Ocean. *Geochimica et Cosmochimica Acta*, 50(7), 1535–1543. [https://doi.org/10.1016/0016-7037\(86\)90327-3](https://doi.org/10.1016/0016-7037(86)90327-3)
- Goldberg, E. D. (1954). Marine geochemistry 1. Chemical scavengers of the sea. *The Journal of Geology*, 62(3), 249–265. <https://doi.org/10.1086/626161>
- Ho, T.-Y., Wen, L. S., You, C. F., & Lee, D. C. (2007). The trace-metal composition of size-fractionated plankton in the South China Sea: Biotic versus abiotic sources. *Limnology & Oceanography*, 52(5), 1776–1788. <https://doi.org/10.4319/lo.2007.52.5.1776>
- Ho, T.-Y., You, C.-F., Chou, W.-C., Pai, S.-C., Wen, L.-S., & Sheu, D. D. (2009). Cadmium and phosphorus cycling in the water column of the South China Sea: The roles of biotic and abiotic particles. *Marine Chemistry*, 115(1–2), 125–133. <https://doi.org/10.1016/j.marchem.2009.07.005>
- Hsu, S.-C., Wong, G., Gong, G. C., Shiah, F. K., Huang, Y. K., Kao, S. J., et al. (2010). Sources, solubility, and dry deposition of aerosol trace elements over the East China Sea. *Marine Chemistry*, 120(1–4), 116–127. <https://doi.org/10.1016/j.marchem.2008.10.003>
- Jacquot, J. E., & Moffett, J. W. (2015). Copper distribution and speciation across the International GEOTRACES Section GA03. *Deep-Sea Research II*, 116(0), 187–207. <https://doi.org/10.1016/j.dsr2.2014.11.013>
- Janssen, D. J., Abouchami, W., Galer, S. J. G., Purdon, K. B., & Cullen, J. T. (2019). Particulate cadmium stable isotopes in the subarctic northeast Pacific reveal dynamic Cd cycling and a new isotopically light Cd sink. *Earth and Planetary Science Letters*, 515, 67–78. <https://doi.org/10.1016/j.epsl.2019.03.006>
- Janssen, D. J., Conway, T. M., John, S. G., Christian, J. R., Kramer, D. I., Pedersen, T. F., & Cullen, J. T. (2014). Undocumented water column sink for cadmium in open ocean oxygen-deficient zones. *Proceedings of National Academy of Sciences*, 111(19), 6888–6893. <https://doi.org/10.1073/pnas.1402388111>
- Janssen, D. J., & Cullen, J. T. (2015). Decoupling of zinc and silicic acid in the subarctic northeast Pacific interior. *Marine Chemistry*, 177(1), 124–133. <https://doi.org/10.1016/j.marchem.2015.03.014>
- John, S. G., & Conway, T. M. (2014). A role for scavenging in the marine biogeochemical cycling of zinc and zinc isotopes. *Earth and Planetary Science Letters*, 394, 159–167. <https://doi.org/10.1016/j.epsl.2014.02.053>
- John, S. G., Helgoe, J., Townsend, E., Weber, T., DeVries, T., Tagliabue, A., et al. (2018). Biogeochemical cycling of Fe and Fe stable isotopes in the Eastern Tropical South Pacific. *Marine Chemistry*, 201, 66–76. <https://doi.org/10.1016/j.marchem.2017.06.003>

- Johnson, K. S., Gordon, R. M., & Coale, K. H. (1997). What controls dissolved iron concentrations in the world ocean? *Marine Chemistry*, 57(3), 137–161. [https://doi.org/10.1016/s0304-4203\(97\)00043-1](https://doi.org/10.1016/s0304-4203(97)00043-1)
- Kim, T., Obata, H., Kondo, Y., Ogawa, H., & Gamo, T. (2015). Distribution and speciation of dissolved zinc in the western North Pacific and its adjacent seas. *Marine Chemistry*, 173, 330–341. <https://doi.org/10.1016/j.marchem.2014.10.016>
- Kim, T., Obata, H., Nishioka, J., & Gamo, T. (2017). Distribution of dissolved zinc in the western and central subarctic North Pacific. *Global Biogeochemical Cycles*, 31, 1454–1468. <https://doi.org/10.1002/2017gb005711>
- Kudo, I., Kokubun, H., & Matsunaga, K. (1996). Cadmium in the southwest Pacific Ocean two factors significantly affecting the Cd–PO₄ relationship in the ocean. *Marine Chemistry*, 54(1), 55–67. [https://doi.org/10.1016/0304-4203\(95\)00100-x](https://doi.org/10.1016/0304-4203(95)00100-x)
- Kuss, J., & Kremling, K. (1999). Spatial variability of particle associated trace elements in near-surface waters of the North Atlantic (30°N/60°W to 60°N/2°W), derived by large volume sampling. *Marine Chemistry*, 68(1–2), 71–86. [https://doi.org/10.1016/s0304-4203\(99\)00066-3](https://doi.org/10.1016/s0304-4203(99)00066-3)
- Lam, P. J., & Bishop, J. K. B. (2008). The continental margin is a key source of iron to the HNLC North Pacific Ocean. *Geophysical Research Letters*, 35, L07608. <https://doi.org/10.1029/2008gl03294>
- Landing, W. M., & Bruland, K. W. (1987). The contrasting biogeochemistry of iron and manganese in the Pacific Ocean. *Geochimica et Cosmochimica Acta*, 51(1), 29–43. [https://doi.org/10.1016/0016-7037\(87\)90004-4](https://doi.org/10.1016/0016-7037(87)90004-4)
- Lane, E. S., Semeniuk, D. M., Strzpek, R. F., Cullen, J. T., & Maldonado, M. T. (2009). Effects of iron limitation on intracellular cadmium of cultured phytoplankton: Implications for surface dissolved cadmium to phosphate ratios. *Marine Chemistry*, 115(3), 155–162. <https://doi.org/10.1016/j.marchem.2009.07.008>
- Li, Y.-H. (1981). Ultimate removal mechanisms of elements from the ocean. *Geochimica et Cosmochimica Acta*, 45(10), 1659–1664. [https://doi.org/10.1016/0016-7037\(81\)90001-6](https://doi.org/10.1016/0016-7037(81)90001-6)
- Liao, W. H., Takano, S., Yang, S. C., Huang, K. F., Sohrin, Y., & Ho, T. Y. (2020). Zn isotope composition in the water column of the northwestern Pacific Ocean: The importance of external sources. *Global Biogeochemical Cycles*, 34, e2019GB006379. <https://doi.org/10.1029/2019gb006379>
- Little, S. H., Vance, D., Siddall, M., & Gasson, E. (2013). A modeling assessment of the role of reversible scavenging in controlling oceanic dissolved Cu and Zn distributions. *Global Biogeochemical Cycles*, 27, 780–791. <https://doi.org/10.1002/gbc.20073>
- Lohan, M. C., Aguilar-Islas, A. M., Franks, R. P., & Bruland, K. W. (2005). Determination of iron and copper in seawater at pH 1.7 with a new commercially available chelating resin, NTA Superflow. *Analytica Chimica Acta*, 530(1), 121–129. <https://doi.org/10.1016/j.aca.2004.09.005>
- Löscher, B. M., De Jong, J. T. M., & De Baar, H. J. W. (1998). The distribution and preferential biological uptake of cadmium at 6°W in the Southern Ocean. *Marine Chemistry*, 62(3–4), 259–286. [https://doi.org/10.1016/s0304-4203\(98\)00045-0](https://doi.org/10.1016/s0304-4203(98)00045-0)
- Mackey, D. J., O'Sullivan, J. E., Watson, R. J., & Dal Pont, G. (2002). Trace metals in the Western Pacific: Temporal and spatial variability in the concentrations of Cd, Cu, Mn and Ni. *Deep-Sea Research I*, 49(12), 2241–2259. [https://doi.org/10.1016/s0967-0637\(02\)00124-3](https://doi.org/10.1016/s0967-0637(02)00124-3)
- Mahowald, N. M., Hamilton, D. S., Mackey, K. R. M., Moore, J. K., Baker, A. R., Scanza, R. A., & Zhang, Y. (2018). Aerosol trace metal leaching and impacts on marine microorganisms. *Nature Communications*, 9(1), 2614. <https://doi.org/10.1038/s41467-018-04970-7>
- Metz, S., Trefry, J. H., & Nelsen, T. A. (1988). History and geochemistry of a metalliferous sediment core from the Mid-Atlantic Ridge at 26°N. *Geochimica et Cosmochimica Acta*, 52(10), 2369–2378. [https://doi.org/10.1016/0016-7037\(88\)90294-3](https://doi.org/10.1016/0016-7037(88)90294-3)
- Middag, R., van Heuven, S. M. A. C., Bruland, K. W., & De Baar, H. J. W. (2018). The relationship between cadmium and phosphate in the Atlantic Ocean unraveled. *Earth and Planetary Science Letters*, 492, 79–88. <https://doi.org/10.1016/j.epsl.2018.03.046>
- Minami, T., Konagaya, W., Zheng, L., Takano, S., Sasaki, M., Murata, R., et al. (2015). An off-line automated preconcentration system with ethylenediaminetriacetate chelating resin for the determination of trace metals in seawater by high-resolution inductively coupled plasma mass spectrometry. *Analytica Chimica Acta*, 854, 183–190. <https://doi.org/10.1016/j.aca.2014.11.016>
- Monteiro, P. M. S., & Orren, M. J. (1985). Trace metals in the Southern Ocean: On the geochemistry of copper. *Marine Chemistry*, 15(4), 345–355. [https://doi.org/10.1016/0304-4203\(85\)90045-3](https://doi.org/10.1016/0304-4203(85)90045-3)
- Morel, F. M. M., Milligan, A. J., & Saito, M. A. (2003). Marine bioinorganic chemistry: The role of trace metals in the oceanic cycles of major nutrients. In H. Elderfield, & K. K. Turekian (Eds.), *The oceans and marine geochemistry* (pp. 113–143). Elsevier-Pergamon. <https://doi.org/10.1016/b0-08-043751-6/06108-9>
- Nishioka, J., & Obata, H. (2017). Dissolved iron distribution in the western and central subarctic Pacific: HNLC water formation and biogeochemical processes. *Limnology & Oceanography*, 62(5), 2004–2022. <https://doi.org/10.1002/lno.10548>
- Noriki, S., & Tsunogai, S. (1992). Directly observed particulate fluxes of Cd, Ni and Cu in pelagic oceans: Implication of two different settling particles. *Marine Chemistry*, 37(1), 105–115. [https://doi.org/10.1016/0304-4203\(92\)90059-j](https://doi.org/10.1016/0304-4203(92)90059-j)
- Price, N. M., & Morel, F. M. M. (1991). Colimitation of phytoplankton growth by nickel and nitrogen. *Limnology & Oceanography*, 36(6), 1071–1077. <https://doi.org/10.4319/lno.1991.36.6.1071>
- Quay, P., Cullen, J., Landing, W., & Morton, P. (2015). Processes controlling the distributions of Cd and PO₄ in the ocean. *Global Biogeochemical Cycles*, 29, 830–841. <https://doi.org/10.1002/2014gb004998>
- Redfield, A. C., Ketchum, B. H., & Richards, F. A. (1963). In M. N. Hill (Ed.), *The influence of organisms on the composition of sea-water in the Sea*. (pp. 26–77). Wiley.
- Roshan, S., DeVries, T., Wu, J., & Chen, G. (2018). The internal cycling of zinc in the ocean. *Global Biogeochemical Cycles*, 32, 1833–1849. <https://doi.org/10.1029/2018gb006045>
- Roshan, S., & Wu, J. (2015a). Cadmium regeneration within the North Atlantic. *Global Biogeochemical Cycles*, 29, 2082–2094. <https://doi.org/10.1002/2015gb005215>
- Roshan, S., & Wu, J. (2015b). The distribution of dissolved copper in the tropical-subtropical north Atlantic across the GEOTRACES GA03 transect. *Marine Chemistry*, 176, 189–198. <https://doi.org/10.1016/j.marchem.2015.09.006>
- Rudnick, R. L., & Gao, S. (2005). Composition of the Continental Crust. In H. D. Holland, & K. K. Turekian (Eds.), *The Crust* (3 ed.), The Crust, Elsevier-Pergamon, 1–64. <https://doi.org/10.1016/b0-08-043751-6/03016-4>
- Saager, P. M., De Baar, H. J. W., & Howland, R. J. (1992). Cd, Zn, Ni and Cu in the Indian Ocean. *Deep-Sea Research A*, 39(1), 9–35. [https://doi.org/10.1016/0198-0149\(92\)90017-n](https://doi.org/10.1016/0198-0149(92)90017-n)
- Sarmiento, J. L., & Gruber, N. (2006). *Ocean Biogeochemical Dynamics*. Princeton University Press.
- Schlitzer, R. (2015). *Ocean data View*. <https://odv.awi.de>
- Schlitzer, R., Anderson, R. F., Dodas, E. M., Lohan, M., Geibert, W., Tagliabue, A., et al. (2018). The GEOTRACES Intermediate Data Product 2017. *Chemical Geology*, 493, 210–223. <https://doi.org/10.1016/j.chemgeo.2018.05.040>
- Sclater, F. R., Boyle, E., & Edmond, J. M. (1976). On the marine geochemistry of nickel. *Earth and Planetary Science Letters*, 31(1), 119–128. [https://doi.org/10.1016/0012-821x\(76\)90103-5](https://doi.org/10.1016/0012-821x(76)90103-5)

- Sherrell, R. M., & Boyle, E. A. (1992). The trace metal composition of suspended particles in the oceanic water column near Bermuda. *Earth and Planetary Science Letters*, *111*, 155–174. [https://doi.org/10.1016/0012-821x\(92\)90176-v](https://doi.org/10.1016/0012-821x(92)90176-v)
- Sunda, W. (2012). Feedback interactions between trace metal nutrients and Phytoplankton in the Ocean. *Frontiers in Microbiology*, *3*, 204. <https://doi.org/10.3389/fmicb.2012.00204>
- Sunda, W. G. (1989). Trace metal interactions with marine Phytoplankton. *Biological Oceanography*, *6*(5–6), 411–442. <https://doi.org/10.1080/01965581.1988.10749543>
- Tagliabue, A., Bowie, A. R., DeVries, T., Ellwood, M. J., Landing, W. M., Milne, A., et al. (2019). The interplay between regeneration and scavenging fluxes drives ocean iron cycling. *Nature Communications*, *10*(1), 4960. <https://doi.org/10.1038/s41467-019-12775-5>
- Takano, S., Tanimizu, M., Hirata, T., & Sohrin, Y. (2014). Isotopic constraints on biogeochemical cycling of copper in the ocean. *Nature Communications*, *5*. <https://doi.org/10.1038/ncomms6663>
- Talley, L. D. (1993). Distribution and formation of North Pacific Intermediate Water. *Journal of Physical Oceanography*, *23*(3), 517–537. [https://doi.org/10.1175/1520-0485\(1993\)023<0517:dafonp>2.0.co;2](https://doi.org/10.1175/1520-0485(1993)023<0517:dafonp>2.0.co;2)
- Talley, L. D., Pickard, G. L., Emery, W. J., & Swift, J. H. (2011). *Descriptive Physical Oceanography: An introduction* (6th ed.). Elsevier
- Treguer, P., Nelson, D. M., van Bennekom, A. J., DeMaster, D. J., Leynaert, A., & Queguiner, B. (1995). The silica balance in the world ocean: A reestimate. *Science*, *268*, 375–379. <https://doi.org/10.1126/science.268.5209.375>
- Twining, B. S., & Baines, S. B. (2013). The trace metal composition of marine Phytoplankton. *Annual Review of Marine Science*, *5*(1), 191–215. <https://doi.org/10.1146/annurev-marine-121211-172322>
- van der Loeff, M. R., Helmers, E., & Kattner, G. (1997). Continuous transects of cadmium, copper, and aluminum in surface waters of the Atlantic Ocean, 50°N to 50°S: Correspondance and contrast with nutrient-like behavior. *Geochimica et Cosmochimica Acta*, *61*, 47–61. [https://doi.org/10.1016/s0016-7037\(96\)00333-x](https://doi.org/10.1016/s0016-7037(96)00333-x)
- Vance, D., De Souza, G. F., Zhao, Y., Cullen, J. T., & Lohan, M. C. (2019). The relationship between zinc, its isotopes, and the major nutrients in the North-East Pacific. *Earth and Planetary Science Letters*, *525*, 115748. <https://doi.org/10.1016/j.epsl.2019.115748>
- Vance, D., Little, S. H., De Souza, G. F., Khatiwala, S., Lohan, M. C., & Middag, R. (2017). Silicon and zinc biogeochemical cycles coupled through the Southern Ocean. *Nature Geoscience*, *10*(3), 202–206. <https://doi.org/10.1038/ngeo2890>
- Wang, R. M., Archer, C., Bowie, A. R., & Vance, D. (2019). Zinc and nickel isotopes in seawater from the Indian Sector of the Southern Ocean: The impact of natural iron fertilization versus Southern Ocean hydrography and biogeochemistry. *Chemical Geology*, *511*, 452–464. <https://doi.org/10.1016/j.chemgeo.2018.09.010>
- Weber, T., John, S., Tagliabue, A., & DeVries, T. (2018). Biological uptake and reversible scavenging of zinc in the global ocean. *Science*, *361*(6397), 72–76. <https://doi.org/10.1126/science.aap8532>
- Whitfield, M., & Turner, D. R. (1987). The Role of particles in regulating the composition of seawater. In W. Stumm (Ed.), *Aquatic surface chemistry* (pp. 457–493). John Wiley & Sons
- Wu, J., & Roshan, S. (2015). Cadmium in the North Atlantic: Implication for global cadmium–phosphorus relationship. *Deep-Sea Research II*, *116*(0), 226–239. <https://doi.org/10.1016/j.dsr2.2014.11.007>
- Wyatt, N. J., Milne, A., Woodward, E. M. S., Rees, A. P., Browning, T. J., Bouman, H. A., et al. (2014). Biogeochemical cycling of dissolved zinc along the GEOTRACES South Atlantic transect GA10 at 40 S. *Global Biogeochemical Cycles*, *28*, 44–56. <https://doi.org/10.1002/2013gb004637>
- Xie, R. C., Galer, S. J. G., Abouchami, W., & Frank, M. (2019). Limited impact of eolian and riverine sources on the biogeochemical cycling of Cd in the tropical Atlantic. *Chemical Geology*, *511*, 371–379. <https://doi.org/10.1016/j.chemgeo.2018.10.018>
- Xie, R. C., Galer, S. J. G., Abouchami, W., Rijkenberg, M. J. A., De Jong, J., De Baar, H. J. W., & Andreae, M. O. (2015). The cadmium–phosphate relationship in the western South Atlantic — The importance of mode and intermediate waters on the global systematics. *Marine Chemistry*, *177*(1), 110–123. <https://doi.org/10.1016/j.marchem.2015.06.011>
- Yang, S.-C., Zhang, J., Sohrin, Y., & Ho, T.-Y. (2018). Cadmium cycling in the water column of the Kuroshio-Oyashio Extension region: Insights from dissolved and particulate isotopic composition. *Geochimica et Cosmochimica Acta*, *233*, 66–80. <https://doi.org/10.1016/j.gca.2018.05.001>
- Yasuda, I. (1997). The origin of the North Pacific intermediate water. *Journal of Geophysical Research*, *102*(C1), 893–909. <https://doi.org/10.1029/96jc02938>
- Yuan, X., & Talley, L. D. (1996). The subarctic frontal zone in the North Pacific: Characteristics of frontal structure from climatological data and synoptic surveys. *Journal of Geophysical Research*, *101*(C7), 16491–16508. <https://doi.org/10.1029/96jc01249>
- Zhang, R., Jensen, L. T., Fitzsimmons, J. N., Sherrell, R. M., & John, S. (2019). Dissolved cadmium and cadmium stable isotopes in the western Arctic Ocean. *Geochimica et Cosmochimica Acta*, *258*, 258–273. <https://doi.org/10.1016/j.gca.2019.05.028>
- Zheng, L., Minami, T., Konagaya, W., Chan, C. Y., Tsujisaka, M., Takano, S., et al. (2019). Distinct basin-scale-distributions of aluminum, manganese, cobalt, and lead in the North Pacific Ocean. *Geochimica et Cosmochimica Acta*, *254*, 102–121. <https://doi.org/10.1016/j.gca.2019.03.038>
- Zheng, L., Minami, T., Takano, S., Minami, H., & Sohrin, Y. (2017). Distribution and stoichiometry of Al, Mn, Fe, Co, Ni, Cu, Zn, Cd, and Pb in seawater around the Juan de Fuca Ridge. *Journal of Oceanography*, *73*(5), 669–685. <https://doi.org/10.1007/s10872-017-0424-2>
- Zheng, L., & Sohrin, Y. (2019). Major lithogenic contributions to the distribution and budget of iron in the North Pacific Ocean. *Scientific Reports*, *9*(1), 11652. <https://doi.org/10.1038/s41598-019-48035-1>